

The late jet in gamma-ray bursts and its interactions with a supernova ejecta and a cocoon

Rongfeng Shen^{1*}, Pawan Kumar^{1*} and Tsvi Piran^{2*}

¹*Department of Astronomy, University of Texas, Austin, TX 78712, USA*

²*Racah Institute of Physics, Hebrew University of Jerusalem, Jerusalem 91904, Israel*

ABSTRACT

Late X-ray flares observed in X-ray afterglows of gamma-ray bursts (GRBs) suggest late central engine activities at a few minutes to hours after the burst. A few unambiguously confirmed cases of supernova associations with nearby long GRBs imply that an accompanying supernova-like component might be a common feature in all long GRB events. These motivate us to study the interactions of a late jet, responsible for a x-ray flare, with various components in a stellar explosion, responsible for a GRB. These components include a supernova shell-like ejecta, and a cocoon that was produced when the main jet producing the GRB itself was propagating through the progenitor star. We find that the interaction between the late jet and the supernova ejecta may produce a luminous (up to 10^{49} erg s⁻¹) thermal X-ray transient lasting for ~ 10 s. The interaction between the late jet and the cocoon produces synchrotron-self absorbed non-thermal emission, with the observed peak X-ray flux density from 0.001 μ Jy to 1 mJy at 1 keV and a peak optical flux density from 0.01 μ Jy to 0.1 Jy (for a redshift $z = 2$). The light curve due to the late jet - cocoon interaction has very small pulse-width-to-time ratio, $\Delta t/t \approx 0.01 - 0.5$, where t is the pulse peak time since the burst trigger. Identifying these features in current and future observations would open a new frontier in the study of GRB progenitor stars.

Key words: gamma-rays: bursts - gamma-rays: theory - supernovae: general

1 INTRODUCTION

Long duration gamma-ray bursts (GRB) – those lasting more than 2 s – are thought to be produced by a relativistic outflow (or jet) with a kinetic energy $\sim 10^{51} - 10^{52}$ erg (beaming effect corrected) when a massive star collapses at the end of its nuclear burning life cycle (see Piran 1999, 2005; Mészáros 2002 for reviews). The massive star origin of GRBs are supported by two different observations: (i) GRBs are found to be in actively star forming galaxies (e.g., Christensen et al. 2004, Castro Cerón et al. 2006) or in star (especially massive ones) forming regions of the host galaxies (e.g., Paczyński 1998; Bloom, Kulkarni & Djorgovski 2002; Fruchter et al. 2006); (ii) for a subset of nearly a dozen of GRBs, X-ray-rich GRBs and X-ray flashes, Supernova (SNa) features – both temporally and spatially associated with the bursts (Woosley & Bloom 2006 for a review) – were detected. For four of those: GRB 980425 (e.g., Galama et al. 1998), 030329 (e.g., Hjorth et al. 2003), 021211 (Della Valle et al. 2003) and 031203 (e.g., Malesani et al., 2004), the physically associated SNe were not only photometrically but also spectroscopically confirmed. The others of the subset show a late-time (~ 10 days) SNa-like “bump” in the optical afterglows,

with a simultaneous strong color evolution, e.g., in GRB 980326 (Bloom et al. 1999) and 011121 (Bloom et al. 2002), consistent with the hypothesis of an underlying SNa.

The *Swift* satellite has recently unveiled a “canonical” behavior pattern in about two-thirds of GRBs’ early X-ray afterglows: a rapid decline phase lasting for $\sim 10^2$ s is followed by a shallow decay phase lasting $\sim 10^3 - 10^4$ s, then by a “normal” power-law decay phase and finally by a possible jet break (Nousek et al. 2006; O’Brien et al. 2006). In addition, X-ray flares are found in about 50% of all *Swift* bursts; they have been discovered in all of the above phases (Burrows et al. 2005, 2007; Chincarini et al. 2007). Even long before *Swift*, a late X-ray flare was detected by BeppoSAX for GRB 970508 (Piro et al. 1998).

In this work we investigate a scenario in which a late jet – responsible for producing the X-ray flares and possibly the shallow decay phase – interacts with other components of a long-GRB stellar explosion. These components include a SNa ejecta, if a SNa explosion is accompanying the GRB event, and a cocoon created by the passage of the main GRB jet through the star (Ramirez-Ruiz et al. 2002, Matzner 2003, Zhang et al. 2004).

In Section 2 we argue for the existence of the late jet and multiple components of a GRB explosion, and provide physical motivations of this work. We investigate the interactions of the late jet with the SNa ejecta in Section 3 and with the cocoon in Section 4

* E-mail: rfshen@astro.as.utexas.edu (RS); pk@astro.as.utexas.edu (PK); tsvi@phys.huji.ac.il (TP)

and calculate their associated emissions. The predicted emissions and their detection prospects are confronted with current observational data in Section 5. The summary and implications are given in Section 6.

2 A MULTI-COMPONENT GRB STELLAR EXPLOSION

Two recently discovered GRB features point to the emergence of a late outflow (jet) after the main γ -ray producing outflow has died. The first is the X-ray flares observed at a few $\times 10^2 - 10^3$ s (as late as $10^4 - 10^5$ s in some cases) after the prompt burst, with a fluence typically about one tenth of the fluence of the prompt γ -rays; in one case, GRB 050502B, this ratio is ~ 1 (Falcone et al. 2007). Lazzati, Perna & Begelman (2008) found that the mean flux of a flare declines with its occurrence time as $\sim t^{-1.5}$. These flares are characterized by a large flux increase and by a very steep rise and decay. Typical increase of the flux ranges from a factor of order unity to 10 and in some rare cases even a few hundred. The decay after the flare peak is as steep as $\propto t^{-4}$, much steeper than the underlying afterglow decay ($\propto t^{-1}$). The pulse width to the peak time ratio $\Delta t/t$ is much smaller than unity, typically ~ 0.3 (Burrows et al. 2005, 2007; Chincarini et al. 2007).

The late flares cannot be due to external-origin mechanisms such as, a density clump in the circumburst medium, or the energy injection into the afterglow blastwave by the trailing slower shells, because the decay slope after the rebrightening from these mechanisms always follows the standard afterglow model, and $\Delta t/t \sim 1$ is always expected (Nakar, Piran & Granot 2003; Nakar & Granot 2007; Lazzati & Perna 2007). They are also unlikely to arise from late collisions between two slow moving shells ejected at same time as the main γ -ray producing shells, since the resultant internal shock is too weak to give rise to the significant emission observed in flares (Zhang 2006). The most likely possibility for X-ray flares is the late activity of the central engine (e.g., Fan & Wei 2005). Such a late activity was proposed already in 1998 as an alternative origin of GRB afterglow (Katz & Piran 1998, Katz, Piran & Sari 1998).

The scenario involving the late engine activity can easily satisfy the constraint that $\Delta t/t \ll 1$. Also in this scenario the late flare is physically separate from the “background” afterglow, so the large amplitude increase of the flux superposed on the decaying afterglow can be naturally explained.

The second feature favoring the existence of a late jet is the shallowly decaying component in the overall X-ray light curve. This component starts at a few $\times 10^2 - 10^3$ s and ends at $10^4 - 10^5$ s during which the flux decays slower than expected for standard decelerating blast-wave afterglow. One straightforward interpretation is that the shallowness is due to an long-lasting energy injection from a late outflow that catches up with the decelerated main outflow (Cohen & Piran 1999; Zhang & Mészáros 2001; Yu & Dai 2007), though there are other possible interpretations for this feature (e.g., Granot & Kumar 2006; Granot, Königl & Piran 2006; Fan & Piran 2006, Panaitescu et al. 2006; Kobayashi & Zhang 2007; Uhm & Beloborodov 2007; Genet et al. 2007).

In those cases where we don’t see a SNa spectroscopically or photometrically in the optical band, we can still hope to explore the existence and properties of the SNa accompanying the GRB by looking at the interaction of a late jet with the SNa remnant and the emission from it. It is likely that every long-duration GRB has a SNa accompanying it but some extrinsic and/or intrinsic bias might have hindered the optical detection of the SNa component (Woosley

& Bloom 2006). A late jet provides a chance to test this picture in the cases where the ordinary SNa features are not easy to detect.

Given the evidences for the existence of a late jet and the physical association of SNe and GRBs, one expects a number of different interactions between the following four components in a GRB event (see Fig. 1 for an illustration): (i) A highly relativistic ($\Gamma \sim 300 - 1000$) narrow jet along the rotation axis with an opening angle ~ 0.1 radian that produces the main GRB event; (ii) A nearly spherically symmetric SNa ejecta moving with speed $\sim 10^4$ km s $^{-1}$; (iii) A cocoon fireball created by the passage of the main GRB jet through the star; (iv) A late relativistic jet responsible for the late X-ray flares after the end of the main GRB. See Woosley & Heger (2006) for a detailed version of the multi-component GRB scenario. Also see Wheeler et al. (2000) for a similar but more detailed model which relates various energetic phenomena such as SNa, GRB and magnetar in a single stellar explosion.

In this work we investigate the interactions of a late jet which might have a similar Lorentz factor and opening angle to those of the main GRB jet, with the expanding SNa ejecta and the cocoon. We assume that the SNa ejecta and the main GRB jet are launched from the central source at about the same time¹. Wheeler et al. (2002) described a similar stellar collapsing scenario where a delayed relativistic jet from the eventually formed black hole catches up and collides with an earlier proto-pulsar toroidal field generated mildly relativistic jet as an origin of the γ -ray burst. Ghisellini et al. (2007) firstly considered the collision between a jetted fireball from an intermittent GRB central engine and a stationary cocoon as an alternative to the standard internal shock scenario, but with higher efficiency. Here we are not attempting to explain how a relativistic jet is formed and a γ -ray burst is produced from the relativistic jet or how an accompanying SNa is generated, rather we are trying to constrain the physical properties of the late jet, SNa ejecta and the cocoon by calculating the emissions from their interactions, and to verify the general picture of GRB-SNa connection.

We will use the following fiducial values for a variety of model parameters. For the late jet, a total energy $E_j \sim 10^{51}$ erg, opening angle $\theta_j \sim 0.1$ radian, LF $\Gamma_j \sim 100$, a delay respective to the launching of the main GRB jet, cocoon and SNa ejecta (in our picture the three are launched at more or less the same time) $t_F \sim 10^2$ s, and a duration $t_{dur} \sim 10^2$ s; for the SNa ejecta, we use an isotropic-equivalent mass $M_{SN} \sim 10 M_\odot$ and speed $V_{SN} \sim 10^9$ cm s $^{-1}$; for the cocoon, we use an energy $E_c \sim 10^{51}$ erg, a terminal LF $\Gamma_c \sim 10$ and an opening angle $\theta_c \sim 0.6$ radian. Nevertheless an appropriate range of numerical values is assigned to each parameter in the real calculation (e.g., E_j could be two orders of magnitude larger or smaller than the fiducial one, cocoon speed could be sub-relativistic and t_F could be as large as $10^4 - 10^5$ s).

The late jet will run into the SNa ejecta first (at a distance $\sim 10^{11}$ cm; see Fig. 2a), and then catches up and run into the cocoon – if it successfully crosses the ejecta – at a larger distance ($\sim 10^{12} - 10^{14}$ cm; see Fig. 2b).

¹ The observational constraint is that GRB and SNa occur within ~ 1 day (e.g., Woosley & Bloom 2006). SNa explosion theories estimate that the SNa shock breaks out at a few tens of seconds after the core rebound (e.g., Janka et al. 2007 and references therein); this time scale is small compared to the delay of the late jet ($t_F \geq 10^2$ s).

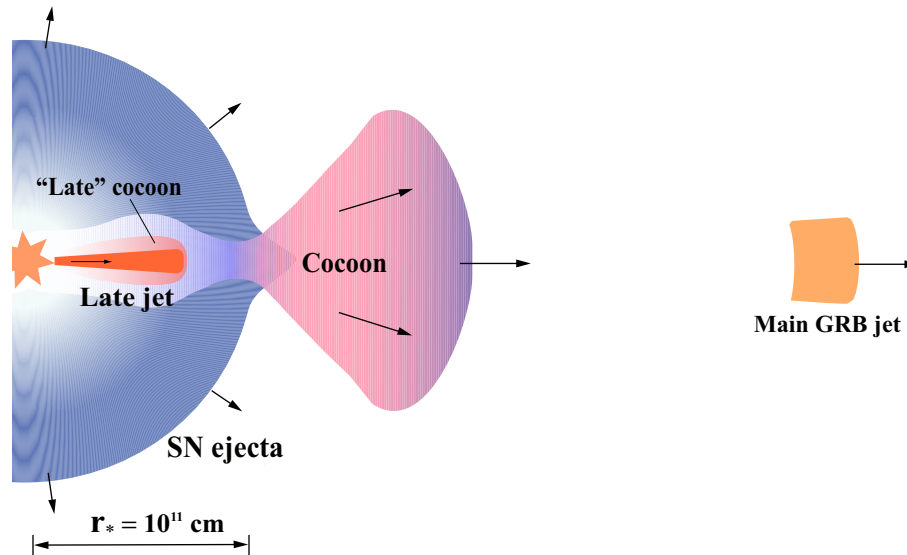


Figure 1. Schematic illustration of multiple components in a long GRB and an accompanying supernova (SNa). An initial, highly relativistic jet, as shown in the right end of the illustration, is responsible for the prompt GRB. A cocoon, that was inflated by the initial GRB jet as the jet was punching through the envelope of the progenitor star, has broken out of the stellar surface at the same time as the main jet, and has accelerated to mildly relativistic speed. A nearly spherically symmetric sub-relativistic ejecta is responsible for the SNa. A late jet responsible for the late X-ray flares in GRBs is launched from the central source and will catch up with the above components. The “late” cocoon is produced when the late jet crosses the SNa ejecta. The distances are not to scale.

3 LATE JET - SNA EJECTA INTERACTION

Since the late jet is highly relativistic and the SNa ejecta is sub-relativistic, the late jet will catch up with the SNa ejecta in a time roughly equal to the distance of the SNa ejecta from the explosion center (where the jet emerged), r_{SN} , divided by light speed c . If the late jet is launched with a delay of t_F , then $r_{SN} \approx V_{SN} t_F \approx 10^{11} V_{SN,9} t_{F,2}$ cm (hereafter we use the convention $X_n = X/10^n$ unless specifically notified). At this time the radial width of the ejecta is about the same size of the initial stellar envelope, $\Delta_{SN} \sim r_* \sim 10^{11}$ cm. The ejecta has hardly moved from the initial position of the progenitor stellar envelope for a jet delay $t_F \sim 100$ s. The particle density in the SNa ejecta is $n_{SN} \simeq 10^{24} V_{SN,9}^{-2} t_{F,2}^{-2} M_{SN,1} \Delta_{SN,11}^{-1} \text{ cm}^{-3}$, where M_{SN} is in units of the solar mass, and it is extremely optically thick. If there is any emission from the interaction between the late jet and the SN ejecta, that emission should be thermal.

3.1 The cavity in the SNa ejecta

We recall that the main GRB jet has already traversed the star and left a cavity in the polar region before the late jet comes. Since the material enclosing the “wall” of the cavity was heated up by the passage of the main jet, it has tendency to refill the cavity. To find out whether the cavity in the SNa ejecta has been filled up before the late-jet encounter, we estimate the time it takes for filling up the cavity.

When inside the star, the cocoon material has a relativistic temperature, i.e., the local sound speed $c_{s,c} = c/\sqrt{3}$. Thus the cocoon material may fill the cavity on a time scale of $r_* \theta_j / c_{s,c} \sim 1$ s, much shorter than the onset of the late jet t_F . However the cocoon will also break out and flow away from the ejecta at that same speed in ~ 10 s, leaving behind a somewhat evacuated polar region. The filling of the polar cavity by the rest of the SN ejecta is uncertain. Assuming a temperature $T \sim 10^8$ K for the SNa-

shocked ejecta material, it has $c_s \sim 1.2 \times 10^8 T_8^{1/2} \text{ cm s}^{-1}$, so the filling time would be $r_* \theta_j / c_s(T) \approx 10^2 r_{*,11} T_8^{-1/2}$ s, comparable to t_F . Considering that the ejecta local temperature possibly decreases from inner parts to outer parts and the transverse size of the cavity gets bigger outward, it is likely that when the late jet hits the ejecta the cavity is partly filled – the inner part is filled but the outer part is not. However, for a very late jet, e.g., $t_F \sim 10^3$ s, the cavity is surely filled before the late jet comes up; and then the question that arises is whether the jet is powerful enough to cross the new refilled cavity. This issue will be discussed elsewhere.

3.2 Late jet - SNa ejecta crossing

The late jet comoving particle density is $n_j = L_j / (\pi \Gamma_j^2 c^3 r_{SN}^2 \theta_j^2 m_p) = 7 \times 10^{16} L_{j,49} \Gamma_{j,2}^{-2} r_{SN,11}^{-2} \theta_{j,-1}^{-2} \text{ cm}^{-3}$, where L_j is the late jet luminosity. Because $n_{SN}/n_j \gg 1$, the late jet will be decelerated to a non-relativistic speed after it first hits the ejecta. It will undergo the same process as the GRB main jet did when propagating through the progenitor star. A cocoon forms in the SNa ejecta and makes a way for the jet head by pushing the ejecta material sideways. To distinguish it from the cocoon associated with the main GRB jet, let us call this cocoon associated with the late jet as the “late cocoon” (see in Figs. 1 and 2a).

When the jet is moving inside the ejecta, the jet head has been slowed down to be at a sub-relativistic speed (Ramirez-Ruiz et al. 2002; Matzner 2003):

$$v_h = \left(\frac{L_j}{\pi r_{SN}^2 \theta_j^2 \rho_{SN} c} \right)^{1/2} \\ = 0.8 \times 10^9 L_{j,49}^{1/2} \theta_{j,-1}^{-1} M_{SN,1}^{-1/2} \Delta_{SN,11}^{1/2} \text{ cm s}^{-1}. \quad (1)$$

Note that if the SNa ejecta width is constant then v_h has no dependence on r_{SN} and therefore on t_F ; but if the SNa ejecta is uni-

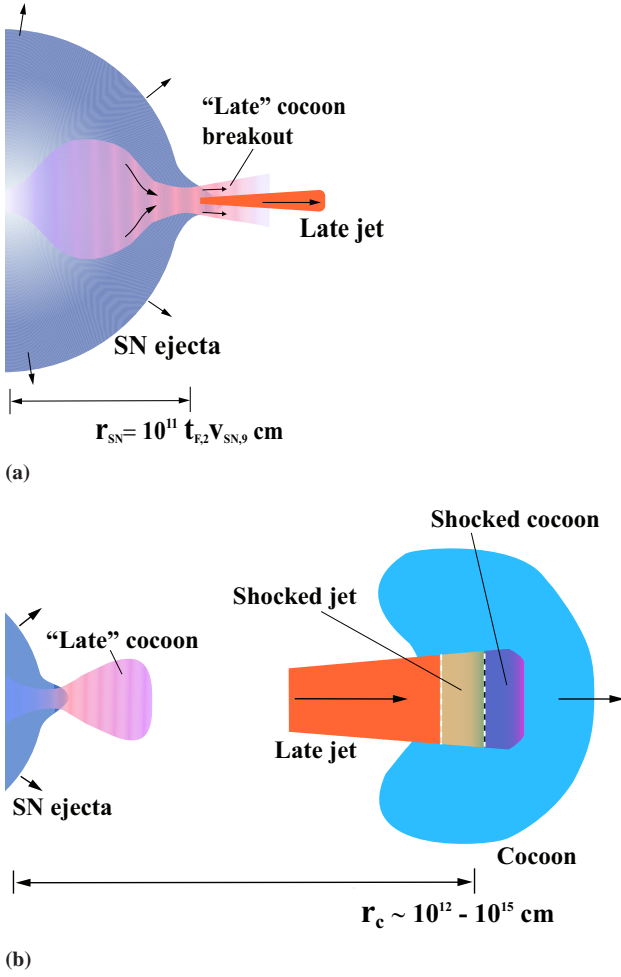


Figure 2. (a): Schematic illustration of the late jet - SNa ejecta interaction, at a slightly later time than shown in Fig. 1. The breakout of the “late” cocoon produces a short thermal emission lasting for ~ 10 s. (b): Schematic illustration of the late jet - cocoon interaction, at a somewhat later time than in (a), when the late jet has completely emerged out of the SNa ejecta and is colliding with the cocoon created by the main GRB jet as it made its way through the progenitor star. A pair of shocks are going through the cocoon and the late jet, respectively. Note that the “late” cocoon has expanded and cooled down at this time.

formly distributed from the centre to the radius r_{SN} , i.e., $\Delta_{SN} \approx r_{SN}$, then v_h increases with t_F as $\propto t_F^{1/2}$. SNa explosion simulations show the latter case, i.e., $\Delta_{SN} \approx r_{SN}$, is the most probable one (e.g., Tanaka et al. 2009).

A constraint on the late jet property can be derived from the requirement that the duration t_{dur} of the jet must be larger than the time that the jet spends to cross the SNa ejecta. Thus $t_{dur} > \Delta_{SN}/v_h$ implies $L_{j,49}^{1/2} t_{dur,2} \theta_{j,-1}^{-1} > 1.2 M_{SN,1}^{1/2} \Delta_{SN,11}^{1/2}$.

3.3 Thermal emission from the late cocoon break out

The late cocoon – formed by the interaction of late jet with SNa ejecta² – will break out of the star immediately following the break-

out of head of the late jet (Fig. 2a). The luminosity of the thermal emission from the late cocoon breakout can be estimated from its temperature and transverse size. Prior to its breakout, the late cocoon has a pressure p_c and its leading head moves with the jet head at the same speed in the radial direction and expands transversely into the SNa ejecta with a speed v_\perp . The ram pressure balance at the lateral interface between the late cocoon and the ejecta material gives

$$p_c = \rho_{SN} v_\perp^2, \quad (2)$$

where ρ_{SN} is the ejecta mass density.

The late cocoon contains an energy E_c that is approximately equal to the jet luminosity L_j times the shell crossing time Δ_{SN}/v_h , and it is radiation pressure dominated. The volume of the late cocoon just before the breakout is $V_c = \pi \Delta_{SN} r_\perp^2 / 3$, where $r_\perp = \Delta_{SN} v_\perp / v_h$ is the transverse size. So the pressure is

$$p_c = \frac{E_c}{3V_c} = \frac{L_j v_h}{\pi \Delta_{SN}^2 v_\perp^2}. \quad (3)$$

Combining with Eq. (2) gives

$$p_c = \left(\frac{L_j \rho_{SN} v_h}{\pi \Delta_{SN}^2} \right)^{1/2}, \quad (4)$$

and the thermal temperature is

$$\begin{aligned} T_{th} &= \left(\frac{3p_c}{a} \right)^{1/4} \\ &= 1.2 \times 10^8 L_{j,49}^{3/16} \theta_{j,-1}^{-1/8} M_{SN,1}^{1/16} r_{SN,11}^{-1/4} \Delta_{SN,11}^{-5/16} \text{ K}, \end{aligned} \quad (5)$$

where Eq. (1) is used. For a late jet with $t_F \sim 10^2$ s, the typical thermal photon energy should be a few keV. T_{th} becomes smaller for larger t_F ; for instance, when the SN ejecta width Δ_{SN} is $\approx r_{SN}$ and, if $L_j \propto t_F^{-1.5}$ (Lazzati et al. 2008), we have $T_{th} \propto t_F^{-0.8}$.

Let us estimate the luminosity of the thermal emission from the late cocoon breakout. The late cocoon transverse expansion speed is

$$\begin{aligned} v_\perp &= \left(\frac{p_c}{\rho_{SN}} \right)^{1/2} \\ &= 0.6 \times 10^9 L_{j,49}^{3/8} \theta_{j,-1}^{-1/4} M_{SN,1}^{-3/8} r_{SN,11}^{1/2} \Delta_{SN,11}^{-1/8} \text{ cm s}^{-1}. \end{aligned} \quad (6)$$

The cocoon transverse size is $r_\perp = \Delta_{SN} v_\perp / v_h = 0.8 \times 10^{11} L_{j,49}^{-1/8} \theta_{j,-1}^{3/4} M_{SN,1}^{1/8} r_{SN,11}^{1/2} \Delta_{SN,11}^{3/8}$ cm. Notice that r_\perp is almost $\sim r_{SN}$ for fiducial parameter values. However, the transverse size of the visible emitting region of the cocoon just at the breakout should be smaller than r_\perp . This is because when the jet head moves near the outer surface of the ejecta, it probably accelerates due to the rapid density drop of the stellar material there; thus the lateral expansion of the cocoon’s leading head immediately following the jet head should be suppressed. Therefore at that time, the overall cocoon might be in an “hourglass” shape, as illustrated in Ramirez-Ruiz et al. (2002) and in our Fig. 2a, rather than a conic shape. At the breakout, the hot cocoon material escapes and accelerates radially from a “nozzle” which has a transverse size on the same order of the jet’s. Thus, the transverse size of the visible emitting cocoon right at the breakout can be estimated as $r_{th,\perp} = r_{SN} \theta_j = 10^{10} \theta_{j,-1} v_{SN,9} t_{F,2}$ cm, while r_\perp should be the transverse size of cocoon at its *widest* cross section.

The luminosity of the black body radiation is

$$\begin{aligned} L_{th} &= \sigma T_{th}^4 \pi r_{th,\perp}^2 \\ &= 4.5 \times 10^{48} L_{j,49}^{3/4} \theta_{j,-1}^{3/2} M_{SN,1}^{1/4} r_{SN,11} \Delta_{SN,11}^{-5/4} \text{ erg s}^{-1}. \end{aligned} \quad (7)$$

² The late cocoon should not be confused with the cocoon that was formed and left behind by the main GRB jet. The latter will be discussed in Section 4.

Using the fact that $L_j \propto t_F^{-1.5}$, one can find this thermal luminosity decreases with t_F as $\propto t_F^{-1.4}$ if $\Delta_{SN} \approx r_{SN}$, or as $\propto t_F^{-0.13}$ if $\Delta_{SN} \sim \text{constant}$. Thus, the radiation efficiency increases as $\propto t_F^{0.1}$ for $\Delta_{SN} \approx r_{SN}$ and as $\propto t_F^{1.4}$ for $\Delta_{SN} \sim \text{constant}$, respectively, which is simply because the emitting transverse area increases with t_F .

This thermal transient will last for a time comparable to the time it takes for the bulk of the late cocoon to escape the ejecta. After that, the luminosity drops quickly due to adiabatic cooling. The late cocoon's outflow speed is $\sim c_s = c/\sqrt{3}$, so the escape time is $\Delta t_{esc} \approx \Delta_{SN}/c_s = 6 \Delta_{SN,11}$ s. Note that L_{th} is large because all the jet power was deposited in the cocoon over a relatively long time (ejecta crossing time $\sim 10^2$ s), and this energy is efficiently radiated away (via black body radiation) within a relatively short time, ~ 6 s.

An even stronger ($L \sim 10^{49}$ erg s $^{-1}$) thermal pulse is associated with the main GRB jet break out. However, this thermal transient is short (~ 10 s), with spectral peak at X-rays, and it happens during the initial stage of the main ‘‘burst’’ γ -ray emission when the X-Ray Telescope (XRT) is not pointing towards the burst. Since this emission can be estimated to be one to two orders of magnitude dimmer than the emission of the burst itself, it is difficult to observe. On the other hand, the thermal transient due to the late cocoon breakout that we consider here arises later and at the time that the XRT is already pointing towards the burst. Hence this transient should be easier to detect.

The fact that we don't observe such thermal transient, preceding flares during the afterglow is somewhat puzzling. If the late jet is fairly early (say, $t_F \leq 10^3$ s), the polar cavity in the SNa ejecta left by the main GRB jet was probably only partially filled, i.e., only the inner part of the cavity is filled (see Sec. 3.1). In that case, the luminosity of the thermal emission would be much smaller than what we estimated above. The situation is more problematic for $t_F \geq 10^3$. We discuss further the observational prospects of this transient in Sec. 5.1.

4 LATE JET - COCOON INTERACTION

We now turn to the interaction of the late jet, after it has successfully crossed the SNa ejecta, with the cocoon that was formed by the main GRB jet (see Fig. 2b). The cocoon breaks out from the star at the same time when the main jet breaks out. Then it accelerates to a mildly relativistic speed. The delay of the late jet with respect to the cocoon breakout is t_F and the late jet catches up with the adiabatically cooled cocoon at $r_i \simeq ct_F/(\beta_j - \beta_c)$, where β_j (Γ_j) and β_c (Γ_c) are the speed (LFs) of the late jet and the cocoon, respectively. When the cocoon speed is mildly relativistic, $r_i \approx 6 \times 10^{14} t_{F,2} \Gamma_{c,1}^2$ cm, which is much further than the late jet - SNa ejecta interaction site. For a sub-relativistic cocoon, r_i is close to but still outside the jet - SNa ejecta interaction region.

4.1 Cocoon geometry and dynamics

At the breakout, the cocoon has an energy E_c , and an energy-to-mass ratio η_c . The cocoon opening angle θ_c is determined by its transverse expansion speed $\sim c/\sqrt{3}$, thus $\theta_c \sim 1/\sqrt{3} = 0.6$. During the early stages of expansion, the cocoon's radial width, Δ_c , is approximately the width of the stellar envelope r_* . Later on, due to the radial expansion of a relativistically moving gas, Δ_c asymptotically approaches $r/(2\Gamma_c^2)$ in the lab frame; this happens when $r \geq r_w \approx r_* \eta_c^2$. The cocoon's LF can be described as

$\Gamma_c(r) \approx \theta_c r/r_*$ when $r < r_s$, and $\Gamma_c \approx \eta_c$ when $r \geq r_s$, where $r_s = \eta_c r_*/\theta_c$ is the saturation radius (Paczynski 1986; Goodman 1986; Shemi & Piran 1990; Piran, Shemi & Narayan 1993; Mészáros, Laguna & Rees 1993). The evolution of the cocoon's comoving volume, $V'_c(r) = \pi \theta_c^2 r^2 \Delta_c \Gamma_c(r)$, is described by

$$V'_c = \begin{cases} \pi \theta_c^3 r^3, & \text{for } r < r_s \\ \pi \theta_c^2 r^2 \eta_c r_*, & \text{for } r_s < r < r_w \\ \pi \theta_c^2 r^3 / (2\eta_c), & \text{for } r > r_w. \end{cases} \quad (8)$$

The pressure evolution of the cocoon follows the adiabatic expansion law: $p_c \propto V_c^{-\gamma}$. Initially the radiation pressure dominates, so $\gamma = 4/3$. When the cocoon's optical depth to Thomson scattering decreases to below unity, the photons decouple from the matter and the radiation pressure drops exponentially; then the gas pressure takes over the dominance of the pressure with $\gamma = 5/3$. The transition happens at radius $r_t = [\sigma_T E_c / (\eta_c m_p c^2 \pi \theta_c^2)]^{1/2} = 3.5 \times 10^{14} E_{c,51}^{1/2} \eta_{c,1}^{-1/2}$ cm, where σ_T is the Thomson scattering cross section. The initial pressure at the breakout is given by

$$p_{c,0} = \frac{E_c}{3V'_c(r_*)} = 5 \times 10^{17} E_{c,51} r_{*,11}^{-3} \text{ dyn cm}^{-2}. \quad (9)$$

The evolution of the cocoon pressure is thus given by

$$\frac{p_c(r)}{p_{c,0}} = \begin{cases} \left(\frac{r_*}{r}\right)^4, & \text{for } r < r_s, \\ \left(\frac{\theta_c}{\eta_c}\right)^{4/3} \left(\frac{r_*}{r}\right)^{8/3}, & \text{for } r_s < r < r_w, \\ (2\eta_c \theta_c)^{4/3} \left(\frac{r_*}{r}\right)^4, & \text{for } r > r_w. \end{cases} \quad (10)$$

The comoving density of the cocoon is assumed to be homogeneous; the same is for the late jet. The width of the late jet is determined by its duration and the radial expansion, so $\Delta_j(r) = ct_{dur} + r/(2\Gamma_j^2)$. The jet comoving density is

$$n_j(r) = \frac{E_{j,iso}}{4\pi r^2 m_p c^3 \Gamma_j^2 (t_{dur} + \frac{r}{2\Gamma_j^2})}. \quad (11)$$

4.2 Cavity in the cocoon

There was also initially a cavity in the cocoon left by the passage of the main jet. Here we estimate how quickly the cavity would be filled. The filling up process starts when the main jet dies off. For a typical duration of GRB $t_{grb} \approx 10$ s, the cocoon has moved to a radius $r_c \approx ct_{grb} = 3 \times 10^{11} t_{grb,1}$ cm. Since $r_c < r_s$, the cocoon gas is still relativistic, the sound speed is $c_s \approx c/\sqrt{3}$, and the time required for cavity to close is $\approx r_c \theta_j / c_s = 0.6 t_{grb,1} \theta_{j,-1}$ s which is $\ll t_F$. Thus the cavity is securely filled when the late jet reaches the cocoon.

Now let us consider a possibility that there is a continuous low-level central engine activity (a *low-power* jet) following the end of the main GRB jet and preceding the late jet. This low-power jet and the late jet more or less are the same phenomenon, only with different energy fluxes. The low-power jet might have too small radiation luminosity to have an observational imprint, however it might still be dynamically important for keeping open the polar cavity in the SNa ejecta and the cocoon.

To keep the cavity open without significant energy dissipation from the jet and cocoon, the transverse pressure, i.e., the thermal pressure, of the low-power jet should be greater than or equal to the cocoon's pressure at r_c . Though the low-power jet started with a high thermal pressure at a distance $r_0 \sim 10^2$ km from the explosion centre where it was launched, at r_c its thermal pressure has dropped to be much smaller than the cocoon pressure because it has adiabatically expanded by a much larger factor than the cocoon

does. Thus, when this low-power jet entered the cavity left by the main GRB jet, it will be squashed rapidly by the gas pressure in the cocoon.

The ram pressure of the low power jet, $p_{j,ram}(r_c) = L_{j,low}/(4\pi r_c^2 c)$ where $L_{j,low}$ is the jet luminosity, can help bore a cavity through the cocoon under suitable conditions. For a long-lasting, continuous jet, the event that takes place after it has been squashed is as follows. If $p_{j,ram}(r_c) > p_c(r_c)$, then the residual, incoming jet will punch a new channel through the cocoon. In doing this, the jet is heated up by the reverse shock, so that the jet which is moving inside the channel could have an enhanced p_j (thermal pressure) that is comparable to p_c , and can keep the channel open. If we assume the low-power jet was launched at the end of the GRB, i.e., $t_{grb} \sim 10$ s, making the equality $p_{j,ram} = p_c(r_c)$ gives $L_{j,low} = 2 \times 10^{48}$ erg s⁻¹, with other parameters at fiducial values. The same equality at later times gives the time dependence $L_{j,low}(t) \propto t^{-2}$. So a decaying luminosity profile $L_{j,low}(t) = 2 \times 10^{48} t_1^{-2}$ erg s⁻¹ for the low-power jet is required to keep the cavity open, i.e., the minimum required total energy for a low-power jet to keep the cavity open is a few $\times 10^{49}$ erg. Note that at this minimal jet luminosity, the process of keeping the cavity open is *not* smooth and a fraction of jet energy is dissipated and it should have some radiation associated with it.

In conclusion, the polar cavity left by the main GRB jet in the cocoon can fill up quickly – before the late jet reaches the cocoon. The presence of a continuous low-power jet can keep this cavity open, provided that the jet has a minimal total energy of a few $\times 10^{49}$ erg. In the following calculation we consider the case when the cavity is filled up. Clearly if the cavity is empty the late jet cocoon interaction is trivial.

4.3 The jet - cocoon interaction phases

The dynamical process of the late jet - cocoon interaction can be decomposed into three phases in the following sequence³: (i) The *Collision Phase* takes place when the jet runs into the cocoon with a forward shock (FS) propagating into the cocoon and a reverse shock (RS) propagating into the jet (see Fig. 2b). (ii) The *Penetration Phase* begins when either the RS crosses the entire jet or the FS crosses the entire cocoon, whichever comes first. In the first case the shocked fluid (RS-shocked jet and FS-shocked cocoon fluid) will decelerate, after RS crosses the jet, when more and more cocoon material are swept by the FS. In the latter case the shocked fluid will be accelerated, after FS crosses the entire cocoon, by the remaining unshocked jet ejecta, and a new particle population will be accelerated at the RS. (iii) The *Expansion Phase* begins when both the FS and RS have run through their courses, and the entire shocked fluid expands adiabatically.

4.3.1 The collision phase

In this phase, the FS propagates into the cocoon and the RS propagates into the jet. For simplicity we approximate the interaction using a planar geometry. The entire jet / cocoon system can be divided into several zones. Outside the FS (RS) front is the unshocked cocoon (jet), and these are taken to be cold plasma, i.e., $e = n$ and $p = 0$, where e , p and n are the fluid energy density (including the

rest mass energy), pressure and particle number density, respectively, all measured in its comoving frame. In between the FS front and the RS front are the shocked cocoon fluid and the shocked jet fluid. These shocked fluids move with the same LF (Γ_s) and have the same thermal pressure; they are separated by a contact discontinuity (CD) plane.

The fluid properties across a shock front are governed by the mass, momentum and energy conservation laws (e.g., Landau & Lifshitz 1959; Blandford & McKee 1976). Across the shock the fluid particle density increases by a factor of $(\hat{\gamma}\bar{\Gamma} + 1)/(\hat{\gamma} - 1)$, and $e = \bar{\Gamma}n$, where $\bar{\Gamma}$ is the shocked fluid LF measured in the unshocked fluid comoving frame; $\hat{\gamma}$ is given by: $p = (\hat{\gamma} - 1)(e - n)$. We use $m_p = c = 1$ to simplify the formulae.

At the CD, the pressure in the shocked jet material equals the pressure in the shocked cocoon material, i.e.,

$$\begin{aligned} (\hat{\gamma}_{RS} - 1)(\bar{\Gamma}_{sj} - 1) \left(\frac{\hat{\gamma}_{RS}\bar{\Gamma}_{sj} + 1}{\hat{\gamma}_{RS} - 1} \right) n_j \\ = (\hat{\gamma}_{FS} - 1)(\bar{\Gamma}_{sc} - 1) \left(\frac{\hat{\gamma}_{FS}\bar{\Gamma}_{sc} + 1}{\hat{\gamma}_{FS} - 1} \right) n_c, \end{aligned} \quad (12)$$

where the subscript ‘‘RS’’ refers to the reverse-shocked fluid and ‘‘FS’’ the forward-shocked one, and $\bar{\Gamma}_{sj}$ and $\bar{\Gamma}_{sc}$ are the shocked fluid LFs measured in the unshocked jet and cocoon comoving frames, respectively. $\hat{\gamma}$ lies between 4/3 and 5/3, and can be written in terms of $\bar{\Gamma}$ as $\hat{\gamma} = (4\bar{\Gamma} + 1)/3\bar{\Gamma}$ (Kumar & Granot 2003). Then Eq. (12) simplifies to

$$(\bar{\Gamma}_{sj}^2 - 1)n_j = (\bar{\Gamma}_{sc}^2 - 1)n_c. \quad (13)$$

Since $\bar{\Gamma}_{sj} = \Gamma_j\Gamma_s(1 - \beta_j\beta_s)$ and $\bar{\Gamma}_{sc} = \Gamma_s\Gamma_c(1 - \beta_s\beta_c)$, we find from the last equation that

$$\Gamma_s = \Gamma_j \frac{\sqrt{a} + \Gamma_c/\Gamma_j}{(a + 1 + 2\sqrt{a}\bar{\Gamma}_{jc})^{1/2}}, \quad (14)$$

where $a = n_j/n_c$ is the density ratio, $\bar{\Gamma}_{jc}$ is the unshocked jet LF measured in the unshocked cocoon rest frame. Note that this expression for Γ_s is valid for both sub-relativistic and relativistic shocks, and for $4/3 \leq \hat{\gamma} \leq 5/3$.

The shock (RS or FS) front moves with a LF different from the LF of the shocked fluid. The shock front LF as measured in the unshocked fluid comoving frame – which we denote as $\bar{\Gamma}_{RS,j}$ for the RS and as $\bar{\Gamma}_{FS,c}$ for the FS – is given by the solution to the shock-jump conditions as a function of $\hat{\gamma}$ and $\bar{\Gamma}$ (Eq. 5 of Blandford & McKee 1976). Using the expression of $\hat{\gamma}$ in terms of $\bar{\Gamma}$, we find

$$\bar{\Gamma}_{RS,j} = \frac{4\bar{\Gamma}_{sj}^2 - 1}{\sqrt{8\bar{\Gamma}_{sj}^2 + 1}}, \quad \text{and} \quad \bar{\Gamma}_{FS,c} = \frac{4\bar{\Gamma}_{sc}^2 - 1}{\sqrt{8\bar{\Gamma}_{sc}^2 + 1}}. \quad (15)$$

These expressions are valid for both sub-relativistic and relativistic shocks.

The pair of shocks exist until one of the two shocks, either the RS or FS, has traversed through the unshocked fluid. From that time on, the interaction will move to the next dynamic phase (*Penetration*). To determine which shock (RS or FS) crossing occurs first, we calculate two radii, r_{RS} and r_{FS} , where r_{RS} is the distance of the system when the RS crosses the rear end of the jet, and r_{FS} is when the FS crosses the front end of the cocoon, pretending that the pair of shocks had existed all the way to the larger of the two radii.

At r_{RS} or r_{FS} , the total distance that the shock has traveled through the unshocked fluid is equal to the radial width of the jet or the cocoon at that radius. Thus the two radii can be obtained by solving the equations

³ The three-phase decomposition treatment follows Dermer (2008) who studied the emission due to the external shocks between a GRB jet and a stationary circumburst dense cloud.

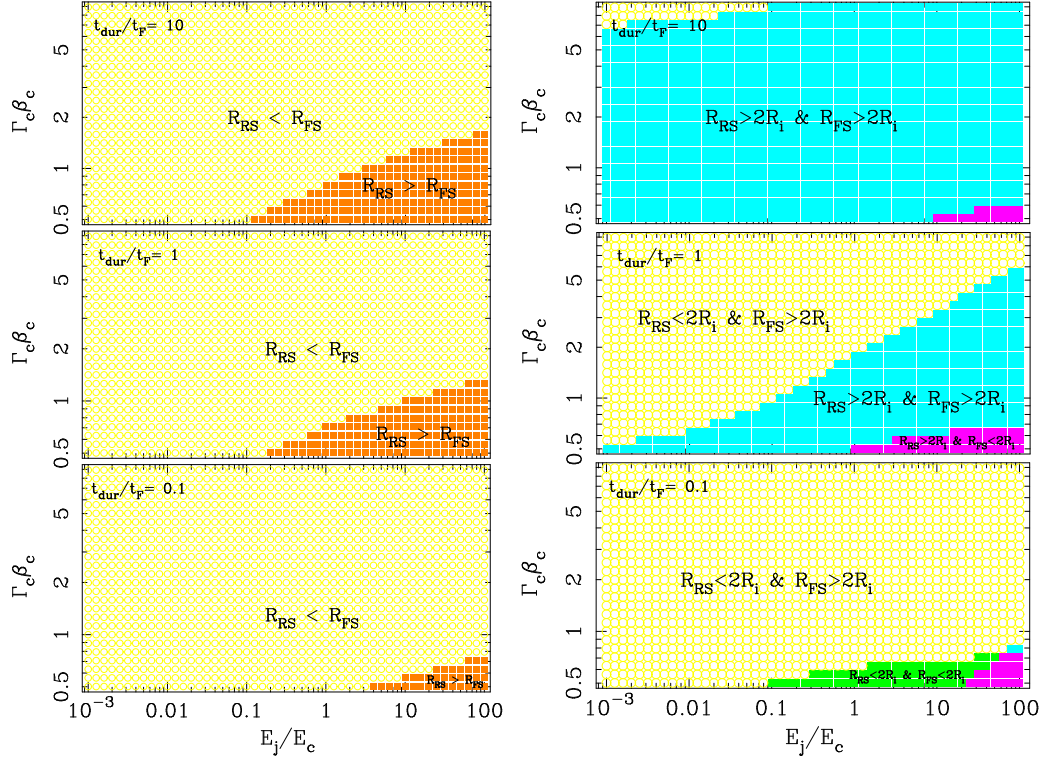


Figure 3. *Left panels:* the comparison between the RS crossing radius r_{RS} and the FS crossing radius r_{FS} in the late jet - cocoon interaction for a set of model parameter space. *Right panels:* the comparison of the two crossing radii with $2r_i$, where r_i is the radius at which the late jet catches up with the cocoon and the interaction begins. Γ_c and β_c are the cocoon’s LF and dimensionless speed, respectively. E_j and E_c are the kinetic energies of the late jet and the cocoon, respectively. Both crossing radii are numerically calculated from Eq. (16). Other parameter values are: $E_c = 10^{50}$ erg, $\theta_j = 0.1$, $\theta_c = 0.6$, $t_F = 300$ s, $\Gamma_j = 100$, $\epsilon_e = 0.1$ and $\epsilon_B = 0.01$. We find the results in this figure do not depend on t_F or Γ_j as long as $t_F \geq 10^2$ s, and $\Gamma_j \gg 1$ (say $\sim 10^2$).

$$\Delta_j(r_{RS}) = \int_{r_i}^{r_{RS}} \frac{(\beta_j - \beta_{RS})}{\beta_j} dr \quad \text{and}$$

$$\Delta_c(r_{FS}) = \int_{r_i}^{r_{FS}} \frac{(\beta_{FS} - \beta_c)}{\beta_c} dr, \quad (16)$$

where we have used $dt = dr/\beta_j \simeq dr/\beta_c$.

If $r_{RS} < r_{FS}$, the RS crosses the jet before the FS crosses the cocoon, and vice versa. We calculate r_{RS} and r_{FS} for different parameters. The results are shown in Fig. 3. We find that $r_{RS} < r_{FS}$, i.e., the RS crossing occurs first, for most of the parameter space; $r_{RS} > r_{FS}$ can only happen when the cocoon bulk motion is sub-relativistic ($\Gamma_c \beta_c < 1$) and the energy carried by the late jet is much larger than that of cocoon ($E_j/E_c \gg 1$). We will use this result later (Sub-sections 4.4 - 4.5) to simplify the calculation of the light curve by assuming that RS crossing always occurs before FS crossing.

4.3.2 The penetration phase

After the RS crosses the jet, the FS continues to pass through the cocoon. We consider the entire shocked fluid, both the old and the newly shocked, moving together with the same LF. In the rest frame of the unshocked cocoon, the LF of the shocked fluid is determined by the equation for the deceleration of a relativistic blast wave in the adiabatic limit as the blast wave sweeps up the stationary ambient medium:

$$\Gamma'_s(x') = \frac{\Gamma'_{s,\Delta}}{\sqrt{1 + 2\Gamma_{s,\Delta}^2 m_c(x')c^2/E'_{j,iso}}} \quad (17)$$

(Böttcher & Dermer 2000) where the prime sign denotes the unshocked cocoon rest frame, $\Gamma'_{s,\Delta}$ is the shocked fluid LF at the end of the collision phase, $m_c(x')$ is the isotropic equivalent swept-up mass at the distance x' that the blast wave has traveled.

A significant deceleration of FS occurs after a point where $\Gamma_{s,\Delta}^2 m_c(x'_d)c^2 = E'_{j,iso}$. Before this point, the FS is coasting into the unshocked cocoon at roughly the same speed it had prior to the RS crossing. After this point, the FS decelerates as it sweeps more and more cocoon material (similar to the external shock scenario for the GRB afterglows). If the FS crossing is earlier than the RS crossing, the process is similar except that it is the RS that continues to travel through the unshocked jet.

4.3.3 The expansion phase

After the FS eventually crosses the entire cocoon, the shocked fluid expands outward with a LF determined by eq. (17) but with $m(x')$ replaced by the isotropic equivalent total mass of the cocoon. The relativistic electrons cool via radiation and expansion. The radiation from an adiabatically expanding relativistic shell, when it is optically thin to the Thomson scattering, is discussed in Barniol Duran & Kumar (2009). We will address the optical thick case in Sec. 4.5.1.

4.4 The emission from the late jet - cocoon interaction

We calculate the emission from the late jet - cocoon interaction, and estimate the flux densities at the optical and X-ray bands using standard shock synchrotron emission (e.g., Sari et al. 1998), and

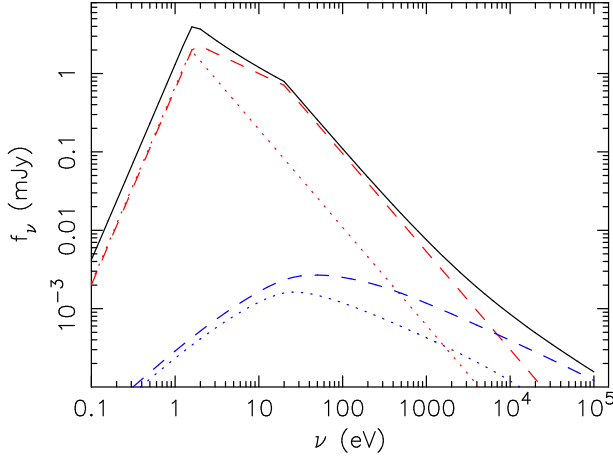


Figure 4. The observed spectrum from the late jet - cocoon interaction at the peak of the light curve for $E_j = E_c = 10^{50}$ erg, $\Gamma_c = 3$, $t_{dur}/t_F = 0.3$ and $z = 2$. Other parameter values are same as in Fig. 3. Various lines represent contributions from different emission regions and spectral components: *red dashed* - RS synchrotron; *red dotted* - RS SSC; *blue dashed* - FS synchrotron; *blue dotted* - FS SSC; *solid* - the sum. For these parameter values, the order of the frequencies is $\nu_c < \nu_{opt} < \nu_a < \nu_i < \nu_X$; ν_{opt} is in the synchrotron-self-absorption optically thick regime, and the spectral peak is around UV band. The SSC emission contribution is important only for γ -ray band and above but is negligible at both optical and X-ray bands.

taking into account the synchrotron self Compton (SSC) radiation. Just behind the shock front, a fraction of the bulk kinetic energy of the fluid upstream, ϵ_e , is transferred to the electrons, and another fraction, ϵ_B , goes to the magnetic field. All the swept-up electrons are shock-heated into a power-law energy distribution with a spectral index p . The minimum LF of shock heated electrons is

$$\gamma_i = \epsilon_e \frac{m_p}{m_e} \left(\frac{p-2}{p-1} \right) (\bar{\Gamma} - 1), \quad (18)$$

where $\bar{\Gamma}$ is the shocked fluid LF measured in the unshocked fluid frame. The magnetic field energy density downstream of the shock front is given by

$$U'_B = \frac{B'^2}{8\pi} = 4\bar{\Gamma}(\bar{\Gamma} - 1)\epsilon_B n_0 m_p c^2, \quad (19)$$

where B' is the comoving frame field strength and n_0 is the particle number density of the unshocked cocoon or jet. The synchrotron characteristic frequency that corresponds to γ_i is

$$\nu_i = \frac{eB'\gamma_i^2\Gamma_s}{2\pi m_e c(1+z)}, \quad (20)$$

where e is the electron charge.

The electron cooling LF, γ_c , is determined by radiative cooling due to synchrotron and SSC radiations:

$$\gamma_c m_e c^2 = \frac{4}{3} \sigma_T \gamma_c^2 U'_B (1+Y) t', \quad (21)$$

where σ_T is the electron's Thomson cross section, t' is the elapsing time in the shocked fluid rest frame, and Y is the Compton parameter defined as the ratio of the SSC to synchrotron luminosities; γ_c is obtained by numerically solving Eq. (21) (e.g., McMahon, Kumar & Piran 2006). Electrons with LF $> \gamma_c$ will cool to γ_e in time t' ; the cooling effect is negligible for electrons with LF $< \gamma_c$. The synchrotron cooling frequency is

$$\nu_c = \frac{\Gamma_s e B' \gamma_c^2}{2\pi m_e c(1+z)}. \quad (22)$$

The self-absorption frequency for the synchrotron electrons, ν'_a , measured in the shocked fluid comoving frame is calculated by (Sari & Piran 1999; Li & Song 2004; McMahon et al. 2006; Shen & Zhang 2009)

$$\max(\gamma_m, \gamma_a) \times 2m_e \nu_a'^2 = F'_{\nu_a'}, \quad (23)$$

where $F'_{\nu_a'}$ is the flux density at ν_a' radiated away from the surface of the shocked region.

The emergent synchrotron spectrum of the shock-heated electrons can be approximated as a piece-wise power law function. The peak of the f_ν -spectrum is at $\nu_{max} = \min(\nu_i, \nu_c)$ and the flux density at the peak is

$$f_{\nu, max} = \frac{N_e}{4\pi D^2} \frac{\Gamma_s m_e c^2 \sigma_T B'}{3e(1+z)}, \quad (24)$$

where N_e is the isotropic equivalent total number of shock-heated electrons, D is the luminosity distance. We also calculate the observed flux density due to SSC by (Rybicki & Lightman 1979)

$$f^{ic}(\nu) = \frac{3}{4} \sigma_T \delta s \times \int \frac{d\nu_s}{\nu_s^2} \nu f^{syn}(\nu_s) \int_{\gamma_i}^{\infty} \frac{d\gamma}{\gamma^2} n_e(\gamma) F\left(\frac{\nu}{4\gamma^2\nu_s}\right), \quad (25)$$

where δs is the line-of-sight width of the emitting source, ν_s and $f^{syn}(\nu_s)$ are the synchrotron frequency and flux density (in the observer frame), respectively, and $n_e(\gamma)$ is the number of shocked electrons per unit volume per unit interval of γ ; $n_e(\gamma) \propto \gamma^{-p}$ for $\gamma > \gamma_i$ [the modification of $n_e(\gamma)$ due to the radiative cooling is included in our calculations]. The function $F(x) = 2x \ln x + x + 1 - 2x^2$ for $0 < x < 1$ and is 0 otherwise. Using the expression for optical depth τ_e due to Thomson scattering, the SSC flux density can be written as

$$f^{ic}(\nu) = \frac{(3/4)\tau_e}{\int_{\gamma_1}^{\infty} n_e(\gamma) d\gamma} \times \int \frac{d\nu_s}{\nu_s^2} \nu f^{syn}(\nu_s) \int_{\gamma_1}^{\infty} \frac{d\gamma}{\gamma^2} n_e(\gamma) F\left(\frac{\nu}{4\gamma^2\nu_s}\right). \quad (26)$$

Fig. 4 depicts the spectrum observed at the time when the RS crosses the jet. The order of the characteristic frequencies in this example is $\nu_c < \nu_{opt} < \nu_a < \nu_i < \nu_X$, and ν_a is in the UV band. The SSC contribution is negligible at optical band and it becomes important for photon energy $\geq \sim 1$ keV.

4.5 Light curves

The light curve from the the late jet - cocoon interaction is mainly determined by the evolution of $f_{\nu, max}$, ν_i , ν_c and ν_a . The optical depth of the shocked fluid region may alter the final light curve shape, which will be addressed later in this sub-section (§4.5.1). We follow the treatment of Yu & Dai (2009) and calculate the light curve. We define T_{exp} as the time when the shocked fluid has traveled a distance of $2r_i$, where r_i is the interaction radius (here and in the following, times denoted with the capitalized letter ‘‘T’’ are the observer’s times and $T = 0$ is the time when the interaction begins). Thus, $T_{exp} = r_i/(2\Gamma_s^2 c)$; before T_{exp} , the increase of the radius can be neglected and B' and Γ_s are considered to be constant; after T_{exp} , the attenuation of the density and B' due to the radius increase must be taken into account.

We also define the shock-crossing time $T_{cro} = \min(T_{RS}, T_{FS})$, where T_{RS} and T_{FS} , calculated in Eq. (16),

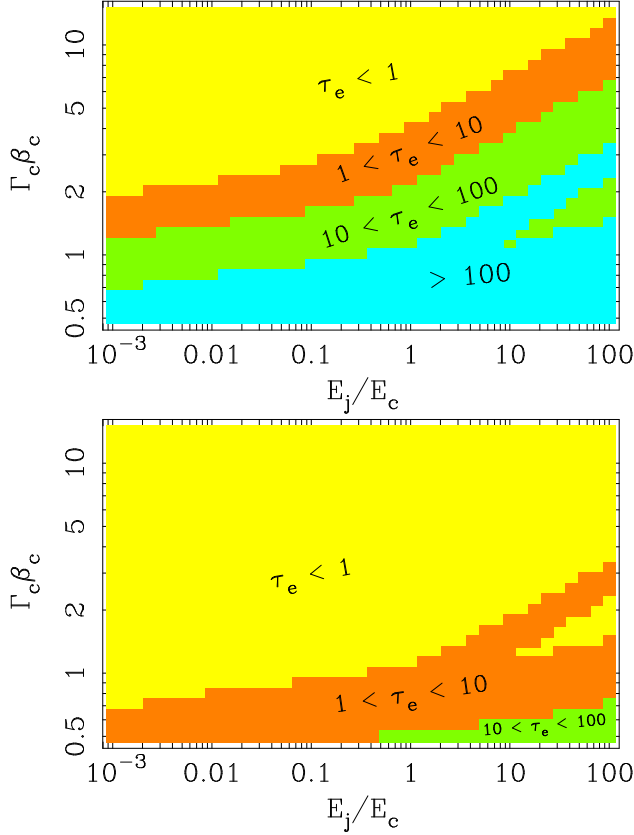


Figure 5. Contours of τ_e — the shocked region optical depth to Thomson scattering at the peak of the flux from the late jet - cocoon interaction. *Top*: for $t_F = 10^2$ s; *Bottom*: for $t_F = 10^3$ s. For even larger t_F (say $\sim 10^4$ s), we find $\tau_e < 1$ for all parameter space. Other parameter values are same as in Fig. 3 except $t_{dur}/t_F = 0.3$.

are the crossing times for the reverse shock and the forward shock, respectively (Fig. 3 shows $T_{RS} < T_{FS}$ for most of the model parameter space). Before T_{cro} , the radial spreading of the shocked region is suppressed by the existence of two shocks, thus the volume of the shocked region $V' \propto r^2$ and the internal energy density $e' \propto V'^{-1} \propto r^{-2}$; the total number of shock heated particles increases linearly with time. After T_{cro} , the radial expansion has to be considered and the shocked region experiences adiabatic cooling. During this phase, $V' \propto r^s$ (where $s = 2 \sim 3$) and the internal energy density $e' \propto V'^{-4/3} \propto r^{-4s/3}$.

Therefore the evolution of B' and $f_{\nu, max}$ are as follows: (i) For $T_{cro} < T_{exp}$,

$$B' \propto \begin{cases} T^0, & T < T_{exp}; \\ T^{-2s/3}, & T > T_{exp}; \end{cases}, \quad (27)$$

$$f_{\nu, max} \propto \begin{cases} T, & T < T_{cro}; \\ T^0, & T_{cro} < T < T_{exp}; \\ T^{-2s/3}, & T > T_{exp}; \end{cases} \quad (28)$$

(ii) For $T_{cro} > T_{exp}$,

$$B' \propto \begin{cases} T^0, & T < T_{exp}; \\ T^{-1}, & T_{exp} < T < T_{cro}; \\ T^{-2s/3}, & T > T_{cro}; \end{cases} \quad (29)$$

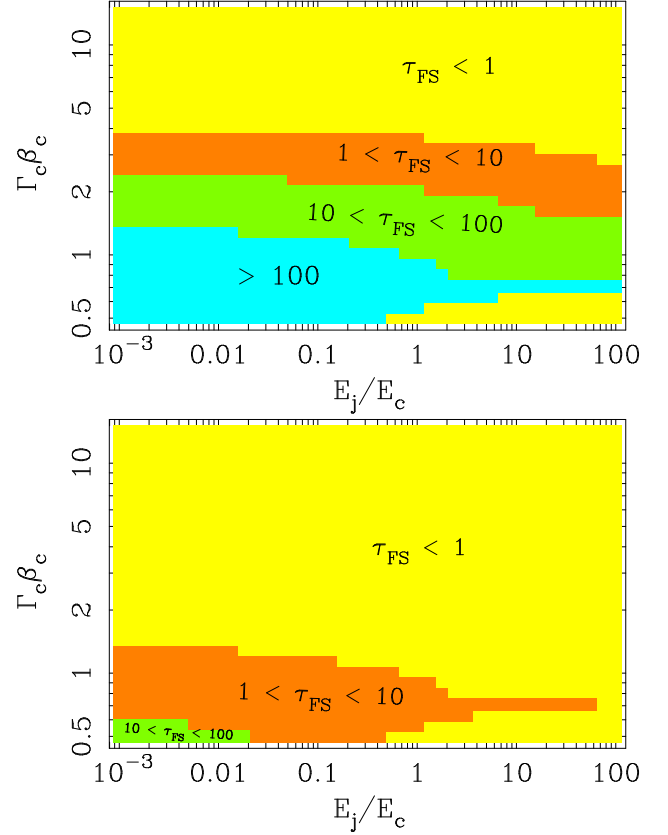


Figure 6. Contours of τ_{FS} — the optical depth for the unshocked cocoon that is still in front of the FS at the peak of the flux from the late jet - cocoon interaction. *Top*: for $t_F = 10^2$ s; *Bottom*: for $t_F = 10^3$ s. For even larger t_F (say $\sim 10^4$ s), we find $\tau_{FS} < 1$ for all parameter space. Other parameter values are same as in Fig. 3 except $t_{dur}/t_F = 0.3$.

$$f_{\nu, max} \propto \begin{cases} T, & T < T_{exp}; \\ T^0, & T_{exp} < T < T_{cro}; \\ T^{-2s/3}, & T > T_{cro}. \end{cases} \quad (30)$$

And the temporal dependences of the characteristic frequencies are given by

$$\nu_i \propto \begin{cases} T^0, & T < T_{exp}; \\ T^{-2s/3}, & T > T_{exp}, \end{cases} \quad (31)$$

$$\nu_c \propto \begin{cases} T^{-2}, & T < T_{exp}; \\ T^{2s-2}, & T > T_{exp}, \end{cases} \quad (32)$$

for $T_{cro} < T_{exp}$, and

$$\nu_i \propto \begin{cases} T^0, & T < T_{exp}; \\ T^{-1}, & T_{exp} < T < T_{cro}; \\ T^{-2s/3}, & T > T_{cro}, \end{cases} \quad (33)$$

$$\nu_c \propto \begin{cases} T^{-2}, & T < T_{exp}; \\ T, & T_{exp} < T < T_{cro}; \\ T^{2s-2}, & T > T_{cro}, \end{cases} \quad (34)$$

for $T_{cro} > T_{exp}$.

Note that the evolution of ν_c given above ignores SSC cooling. SSC cooling is included in our numerical calculation as described by Eq. (26). We find that the resultant ν_c scalings are not very different from those given above.

To calculate the light curve, we first calculate B' , $f_{\nu, max}$, ν_i ,

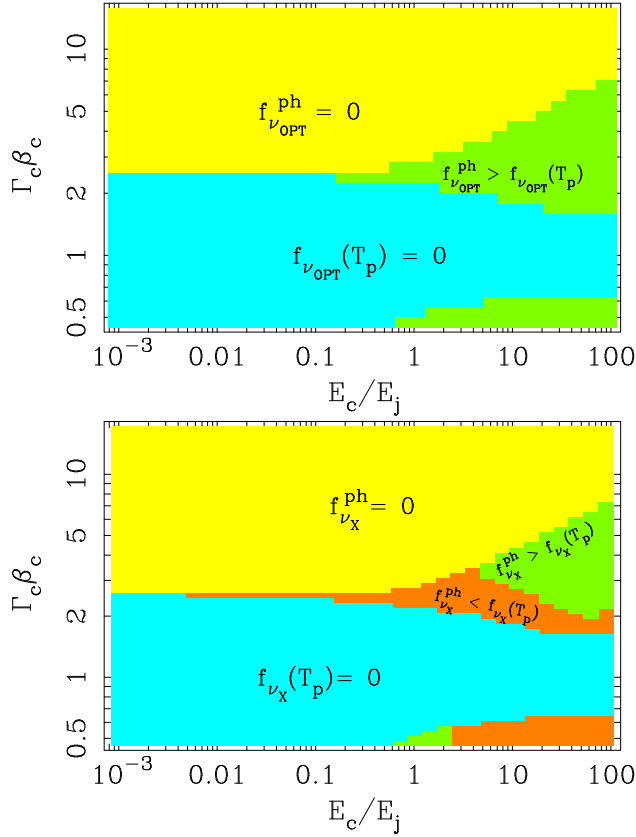


Figure 7. The comparison between the observed in situ flux density at T_p and the photospheric flux density, at the optical (*top*) and X-ray (*bottom*) bands, respectively. The photospheric flux is meaningful only in cases of $(\tau_e + \tau_{FS}) > 1$ at T_p ; those cases where $(\tau_e + \tau_{FS}) < 1$ are marked with $f_{\nu}^{ph} = 0$. In cases of $\tau_{FS} > 1$, the emission produced at T_p is undetectable, and the light curve is dominated by photosphere emission arriving at a later time; these cases are marked with $f_{\nu}(T_p) = 0$. When $\tau_e > 1$ and $\tau_{FS} < 1$, the light curve is dominated by either the in situ emission produced at T_p and diminished by a factor of τ_e or the photospheric emission, whichever is larger, so is the observed peak flux.

ν_c and ν_a at the expected peak time $T_p = \min(T_{cro}, T_{exp})$, then we use the temporal evolution of B' and $f_{\nu, max}$ to get the observed flux density at other times. The SSC contribution to the flux is included in the light curve calculation. In addition, the optical thickness of the late jet - cocoon system to Thomson scattering could alter the light curve shape because it could delay the escape of the photons from the system; we will consider this next, and then discuss the light curve results.

4.5.1 Optically thick cocoon

When r_i is small – either because of a low LF of the cocoon or a small t_F – the cocoon could be optically thick to Thomson scattering. For instance, the optical depth of the entire cocoon at r_i is estimated to be $\approx 2\sigma_T E_c / [4\pi r_i^2 \Gamma_c m_p c^2 (1 - \cos\theta_c)] \sim 0.1 E_{c,51} \Gamma_{c,1}^{-5} t_{F,2}^{-2}$. Figs. 5 and 6 depict the calculated τ_e and τ_{FS} – the optical depths of the shocked region and the unshocked cocoon, respectively – at the expected light curve peak time T_p .

When $\tau_e \gg 1$, the photons are subject to numerous scattering (diffusion) before escaping the plasma. The emergent flux is spread over the diffusion time scale

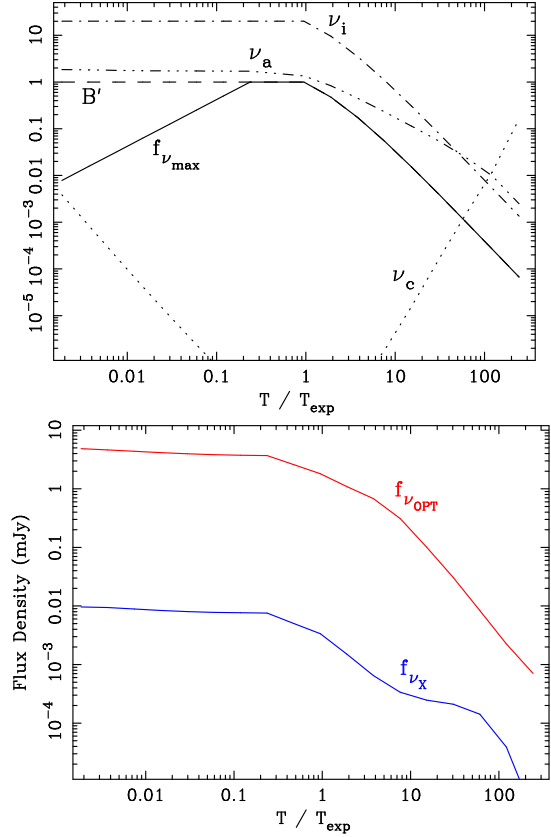


Figure 8. *Top:* temporal evolutions of B' , ν_i , ν_c , ν_a and $f_{\nu, max}$ during the late jet - cocoon interaction for same model parameter values as in Fig. 4. ν_i , ν_c and ν_a are in units of eV, whereas B' and $f_{\nu, max}$ are normalized by their maximum values, respectively. *Bottom:* observed light curves in optical and X-ray bands. The observer's time T is normalized by the expansion time scale $T_{exp} = r_i / (2\Gamma_s^2 c)$ and $T = 0$ is when the interaction begins.

$$\Delta T_d \approx \frac{r_{ph}}{2\Gamma_s^2 c}, \quad (35)$$

which is the delay between the actually observed time of a photon and the time it would have been observed in the absence of scattering, where r_{ph} is the photosphere radius.

When $\tau_e \gg 1$, we consider all the photons emitted during the time up to T_p as a photon gas co-expanding with the baryon gas; the expansion of the system is governed by the radiation pressure rather than the gas pressure, and the scattering between photons and electrons is nearly elastic. This treatment is different from the one adopted by Pe'er, Meszaros & Rees (2006) who consider the case where the gas pressure dominates over the radiation pressure and photons Compton scatter off thermal electrons.

The equation of state for the photon gas is $(h\nu)^4 \propto V^{-4/3}$, where $h\nu$ is the characteristic photon energy and $V \propto r^2 \Delta_c$ is the volume of the system (in the photon-baryon gas co-expanding phase, the LF of the system is constant). The width of the system Δ_c is $\propto r$ for the thin shell case and is constant for the thick shell case. Since the system is shock-compressed after the collision, we believe the thin shell case is a more likely possibility to consider than the thick shell case. Thus the temporal evolution of the photon energy is $h\nu \propto T^{-1}$, where T is the observer's time. The shape of the spectrum at the photosphere is unchanged from that at the time T_p .

We first calculate the flux density at T_p neglecting all optical-thick effects. If $\tau_e > 1$ and $\tau_{FS} < 1$, the promptly observed flux

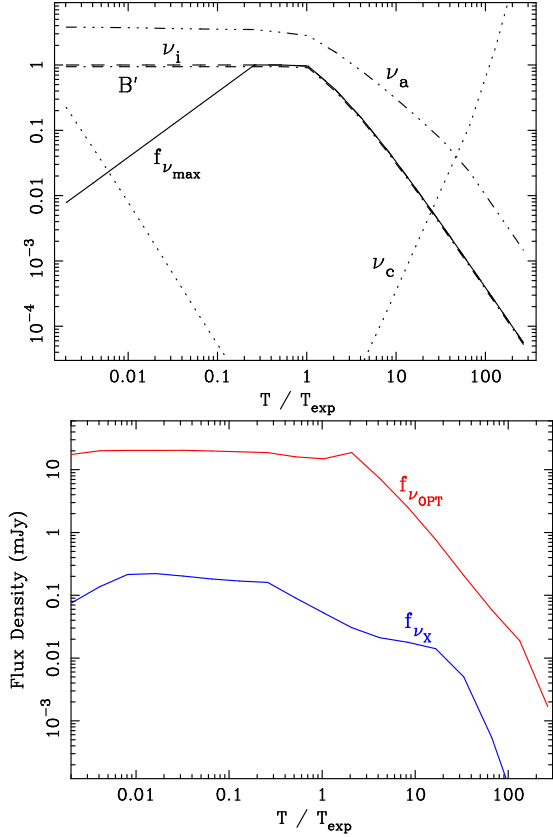


Figure 9. *Top:* same as Fig. 8 but for $E_j = 10 \times E_c = 10^{51}$ erg and $\Gamma_c = 5$. *Bottom:* observed light curves. Both the optical and X-ray light curves show a flat part at $T < T_{exp}$ because both frequencies are in the fast cooling regime and the decrease of $\nu_c \propto T^{-2}$ just compensates for the increase of $f_{\nu,max} \propto T$. The optical peak at $T > T_{exp}$ is due to the fact that ν_c increases steeply and ν_a drops below ν_{opt} . A rise does not show up in the X-ray light curve at $T > T_{exp}$ because ν_X is always above all of ν_a, ν_i and ν_c .

in situ at T_p is $1/\tau_e$ of that calculated when τ_e is neglected. Then we also calculate the emergent flux at the photosphere. The real peak flux of the light curve is either the observed flux in situ at T_p or the photospheric flux at later time, whichever is larger. and the light curve would be dominated by that larger component. In case the observed flux in situ at T_p is stronger than the photospheric flux, we calculate elaborately the light curve shape following T_p in the way described in Sec 4.5 and numerically estimate its peak time and pulse width. In case the observed light curve is dominated by the flux at the photosphere, its peak time is the photospheric time $T_{ph} \sim r_{ph}/(2\Gamma_s^2 c)$ and the pulse width is also $\approx T_{ph}$. If $\tau_{FS} > 1$, then the unshocked cocoon blocks the light produced in the shocked region from reaching the observer, thus the emission at the photosphere is what we actually see only and it will completely dominate the light curve. We show in Fig. 7 a comparison between the observed flux in situ at T_p and the photospheric flux for the considered model parameter space.

4.6 Results

Figs. 8 - 10 depict the light curves and the temporal evolutions of emission properties for different values of model parameters. Initially the light curve remains constant up to the shock crossing time or the expansion time, whichever is smaller. This is because

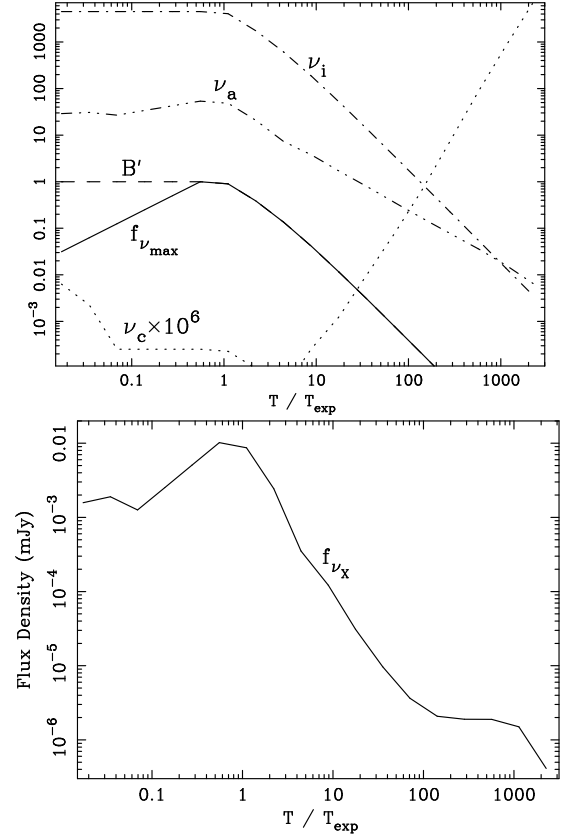


Figure 10. *Top:* same as Fig. 8 but for $E_j = 10^2 \times E_c = 10^{52}$ erg and $\Gamma_c \beta_c = 0.5$. *Bottom:* observed light curve in X-rays. The optical light curve is not shown, because for this set of parameter values the cocoon is extremely optically thick ($\tau_e \gg 1$ and $\tau_{FS} = 0$; see Fig. 5 and 6), and we find the optical light curve is dominated by the photosphere emission, whose numerical light curve shape has to be calculated differently from that in the optically thin case. However in the X-ray band, the prompt non-thermal flux, after diminished by the optical thick effect, is still brighter than the later photospheric flux. Thus we use the diminished prompt non-thermal flux to represent the observed X-ray light curve.

$\nu_c < \nu_{opt}$, and therefore the increase of $f_{\nu,max}$ is compensated by the decrease of ν_c . Later, the X-ray flux decays due to the adiabatic expansion, while the optical flux continues to rise as long as $\nu_{opt} < \nu_a$. Therefore generally the optical pulse peaks later and is wider than the X-ray pulse.

The peak flux density distributions are presented in Fig. 11. For the range of model parameter values, i.e., $E_j/E_c = 10^{-2} - 10^2$, $\Gamma_c \beta_c = 0.5 - 20$, $\epsilon_B = 10^{-2} - 10^{-4}$, $t_F = 10^2 - 10^4$ s and $E_c = 10^{50}$ erg, the optical peak flux density $f_{\nu_{opt}}$ ranges from $\sim 0.01 \mu\text{Jy}$ to ~ 0.1 Jy, and the X-ray peak flux density is $f_{\nu_X} \approx 0.001 \mu\text{Jy} - 1 \text{ mJy}$ for $z = 2$. For typical parameter values, i.e., $E_j/E_c = 10^{-1}$, $\Gamma_c \beta_c = 3$, $\epsilon_B = 10^{-2}$ and $t_F = 10^2$ s, the fluxes are $f_{\nu_{opt}} \sim 0.1$ mJy, $f_{\nu_X} \sim 1 \mu\text{Jy}$. The ratio of the peak flux densities at optical and X-rays is roughly constant: $f_{\nu_{opt}}/f_{\nu_X} \sim 10^2$, since the optical band is much closer to the spectral peak than the X-rays. The peak flux density is highest for $\Gamma_c \approx 5 - 10$, i.e., when the cocoon is mildly relativistic.

The peak flux densities have very broad ranges. The higher ends of the ranges are high compared to the afterglows, but they correspond to some certain extreme model parameter value (i.e., $E_j/E_c \sim 10^2 - 10^3$) and higher values among model parameter ranges (e.g., $\Gamma_c \sim 5 - 10$). The flux values corresponding to typ-

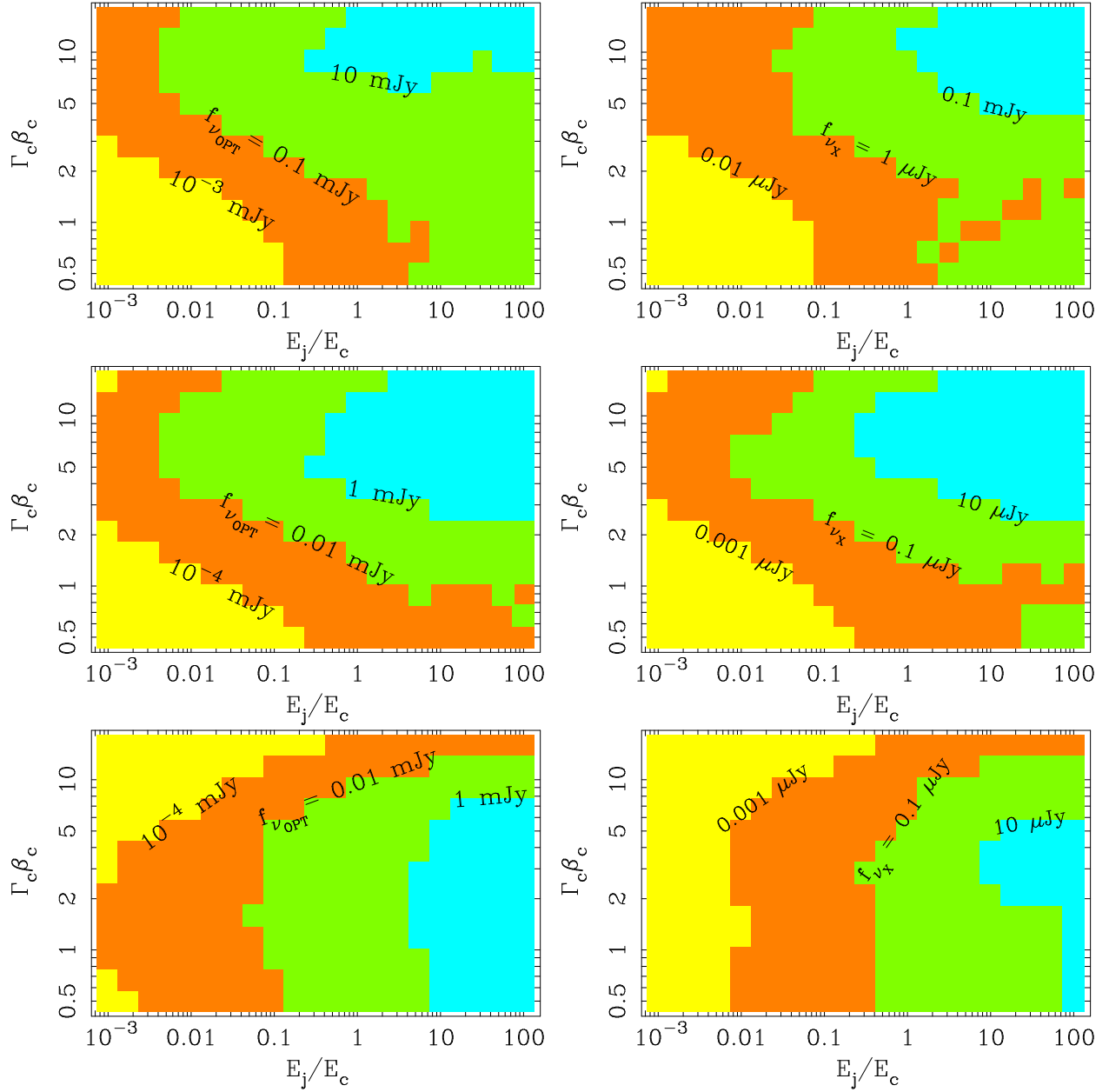


Figure 11. The contours of the observed peak flux densities from the late jet - cocoon interaction. *Left panels:* at the optical band ($\nu = 2$ eV). *Right panels:* at the X-ray band ($\nu = 1$ keV). The flux density values labeled on the contours are the demarcation values for two neighbouring contour belts. The ratio of the late jet's duration over its delay t_{dur}/t_F is 0.3 and the redshift is $z = 2$. *Top panels:* for $t_F = 10^2$ s; other parameter values are same as in Fig. 3. *Middle panels:* same as in top panels except for $\epsilon_B = 10^{-4}$. *Bottom panels:* same as in top panels except for $t_F = 10^4$ s.

ical model parameter values are comparable to those of observed afterglows (see Figs. 17 - 18).

Fig. 11 also shows the dependence of peak flux densities on ϵ_B and t_F . When ϵ_B varies from 10^{-2} to 10^{-4} , f_ν decreases by a factor of ~ 10 . This reflects the fact that synchrotron electrons' peak specific radiation power and characteristic frequencies are all linearly dependent on B' . When t_F increases from 10^2 s to 10^4 s, f_ν drops by a factor of $\sim 10^2$. This is because the interaction radius $r_i \propto t_F$ and therefore both the cocoon and jet densities are smaller at r_i and so is B' for a larger t_F . However for $\Gamma_c \beta_c < 2$, f_ν increases for a larger t_F ; this is due to the optical thickness when t_F is small (see Sec. 4.5.1).

Figs. 12 and 13 show the distribution of peak times of the light

curves, according to which the peak time can be approximated by t_F , particularly for large values of t_F . We measure the full width at half maximum (FWHM) of the light curves to characterize the pulse width, whose distribution is shown in Figs. 14 and 15. The ratio of the pulse width to the peak time, $\Delta t/t$, has a broad range of 0.01 - 0.5; typically, for lower $\Gamma_c \beta_c$ or E_j/E_c , pulses are wider. The optical pulses are often wider than X-ray pulses, but the difference is not large.

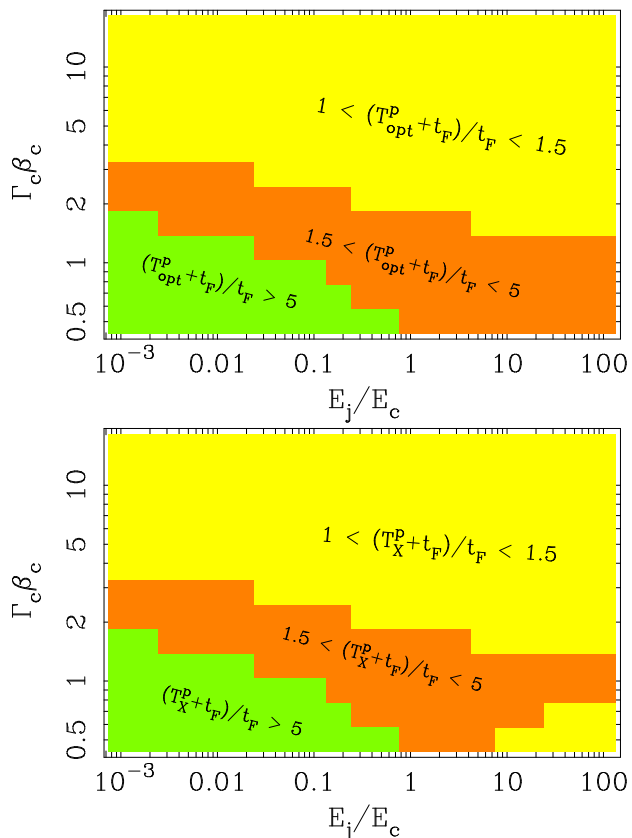


Figure 12. Contours of the light curve peak time for the emission from the late jet - cocoon interaction, since the burst trigger and normalized by the delay time of the late jet. *Top*: for the optical light curve; *Bottom*: for the X-ray light curve. Model parameter values are $t_{dur}/t_F = 0.3$ and $t_F = 100$ s. Other parameter values are same as in Fig. 3.

5 OBSERVATIONAL IMPLICATION AND DETECTION PROSPECTS

5.1 The Late jet - SNa ejecta interaction

We find that late jet - SNa ejecta interaction produces a thermal transient due to the breakout of a “late” cocoon produced by the late jet crossing the SNa ejecta. Thermal X-ray emission was detected from X-Ray Flash (XRF) 060218 (Campana et al. 2006). But its long lasting, slowly variable light curve suggests that it originated in the shock breakout of a quasi-spherical, mildly relativistic ejecta and the late jet scenario does not apply to this event. For the prevailing X-ray flares detected in GRBs, spectral fit shows no compelling evidence for a thermal component (Falcone et al. 2007).

The non-detection of a thermal X-ray transient in GRBs with flares indicates that the late jet - SNa ejecta interaction is weak or non-existent. There are three possible reasons for the non-detection: (i) The cavity in the polar region of the progenitor star created by the main GRB jet is still open, and in that case the interaction between the late jet and the partially filled cavity is weak resulting in a significantly lower signal than we have estimated in Sec. 3.3. The cavity can be kept open, either because the time was too short for the cavity to fill up, or due to a continuous, low-power jet that precedes the late jet. This low-power jet might also keep the cavity in the cocoon open (see Section 4.2). (ii) The cocoon that is in front of the “late” cocoon and the late jet could be optically thick, e.g., $\tau_c \sim 0.1 E_{c,51} \Gamma_{c,1}^{-5} t_{F,2}^{-2}$ (also see Figs. 5 - 6), and

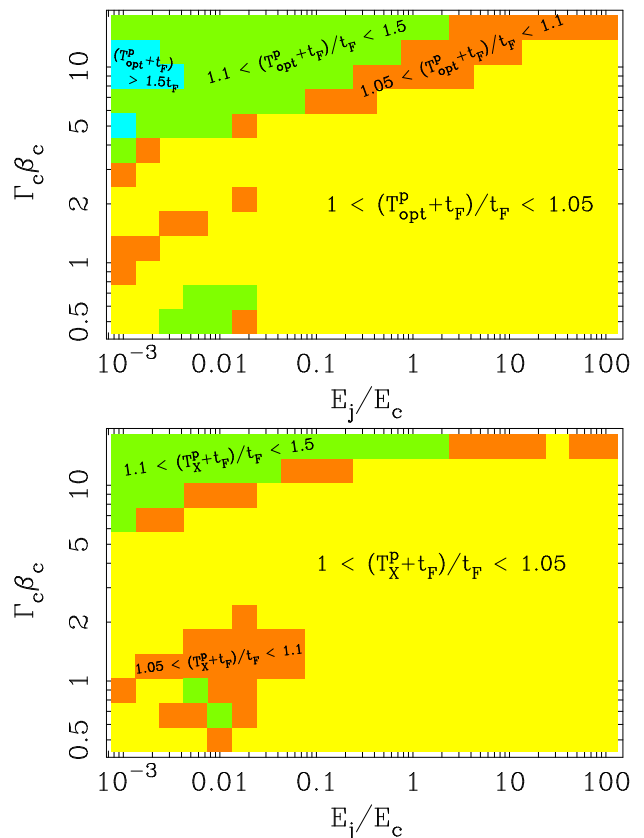


Figure 13. Same as Fig. 12 except for $t_F = 10^4$ s.

block the thermal transient signal. (iii) It is also possible that even though the GRB was associated with the death of a massive star the stellar envelope collapsed producing no supernova at all. In the failed SN explosion the whole stellar envelope would collapse on a free-fall time scale of a couple of hundred seconds (see, e.g., Kumar, Narayan & Johnson 2008), form a torus and then be accreted. Note that even in this extreme situation, the cocoon associated with the main jet should still exist because the cocoon is created when the head of the prompt GRB jet passes through the stellar envelope, long before the envelope reacts to the core collapse.

5.2 Late jet - cocoon interaction

A schematic sketch of light curves due to emission from the late jet - cocoon interaction, superposed on the underlying external-shock afterglow component, is illustrated in Fig. 16. The expected emission from late jet - cocoon interaction has the following features:

(1) *Peak flux density.* The peak flux has a broad distribution (see Fig. 11). Except for the cases of a very slow cocoon or a very low jet-to-cocoon energy ratio, the emission is fairly bright. For instance, the range of the calculated X-ray peak flux densities corresponds to a flux in the 0.3–10 keV band of $\approx 10^{-14} - 10^{-8}$ erg $s^{-1} cm^{-2}$ (for a spectral index $\beta_X = -1.1$) while the Swift / XRT sensitivity is 2×10^{-14} erg $s^{-1} cm^{-2}$ in 10^4 s (Gehrels et al. 2004). Therefore, the X-ray emission from this interaction is detectable by Swift / XRT for most of the parameter space.

(2) *A small $\Delta t/t$ (< 0.5 ;* see Figs. 14 and 15).

(3) *A non-thermal spectrum.* The emission is mostly non-thermal, except when the cocoon speed is sub-relativistic and the delay of the late jet is small (e.g., $t_F \lesssim 10^3$ s) thus the thermal

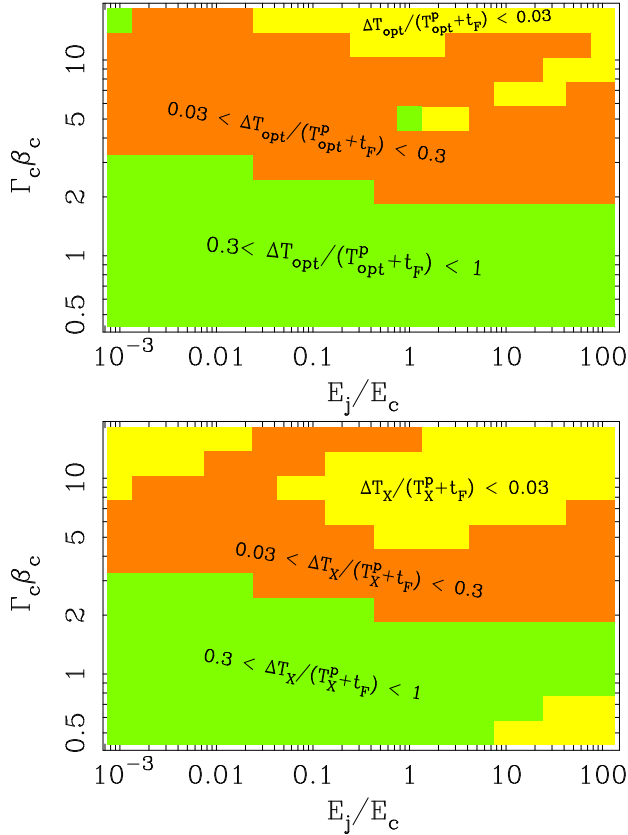


Figure 14. Contours of the full width at half maximum (FWHM) of the light curve from the late jet - cocoon interaction, normalized by the peak time of the light curve since the burst trigger. *Top*: for the optical light curve; *Bottom*: for the X-ray light curve. Model parameter values are $t_{dur}/t_F = 0.3$ and $t_F = 100$ s. Other parameter values are same as in Fig. 3.

photospheric emission might dominate. The X-ray band is in the “fast cooling” spectral regime when the emission is non-thermal, and the optical is near the synchrotron self absorption frequency. The flux density ratio of optical and X-ray is roughly $\sim 10^2$ for $p = 2.5$ (this ratio is larger for larger values of p). This implies that whenever a X-ray pulse is observed, we expect to see an accompanying increase of the optical flux.

Could some of the late X-ray flares in GRBs originated from the late jet - cocoon interaction? We compare the properties of these flares with the prediction of our calculations in the following.

(1) The observed peak count rate in the XRT band (0.3 - 10 keV) for flares is distributed over the range of 0.1 - 100 counts s^{-1} (Chincarini et al. 2007). Using the empirical instrument conversion factor this translates to $f_{\nu_X} \approx 1\mu\text{Jy} - 1\text{mJy}$. This range for the observed X-ray flare flux is roughly what is expected for the late jet - cocoon interaction (cf. Fig. 11).

(2) The observed value for $\Delta t/t$ lies in the range of 0.02 to 0.6, with a mean value of XRT band (0.3 - 10 keV) 0.1 (Chincarini et al. 2007). This range is consistent with our calculation (see Figs. 12 and 13).

(3) It is rare to find an optical flare accompanying a X-ray flare. This is in part due to the fact that very few simultaneous optical observations were made in most cases. Nevertheless, we do find four cases where an optical flare or rebrightening is reported and the X-ray data during the time either is missing or does show a flare. These four cases – GRB 050904 (shows an optical flare but its X-ray coverage was too sparse to identify a simultaneous flare; Boër et

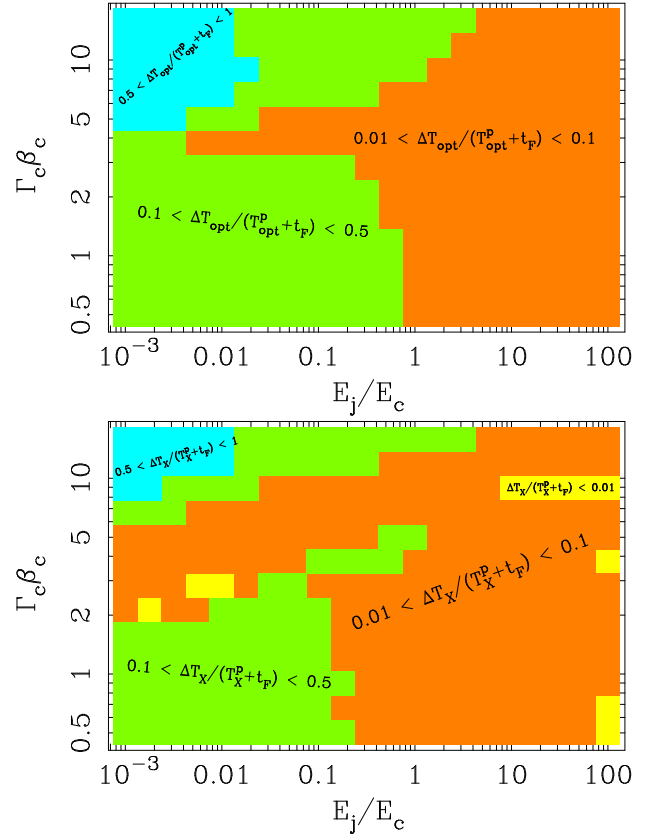


Figure 15. Same as Fig. 14 except for $t_F = 10^4$ s.

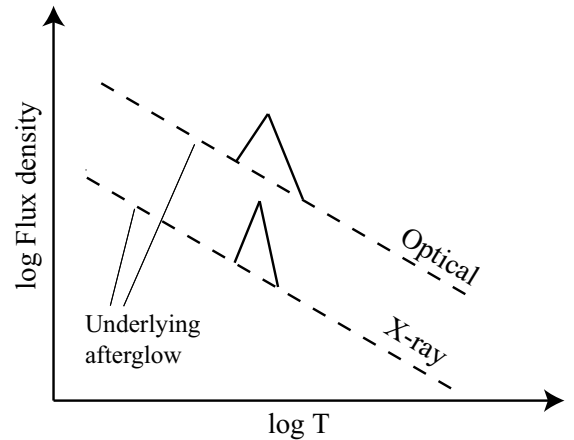


Figure 16. The schematic light curve for the emission from the late jet - cocoon interaction superposed on the underlying afterglow light curve. Note the zero time in this figure is the burst trigger time, different from the zero times in Figs. 8 - 10.

al. 2006), 060206 (Stanek et al. 2007; Woźniak et al. 2006), 060210 (Stanek et al. 2007; Curran et al. 2007) and 080129 (Greiner et al. 2009) – are shown in Fig. 17. The last burst shows an early optical flare but without a simultaneous X-ray coverage, and a very late (2×10^5 s since trigger) rebrightening in both optical and X-rays. Among them, the achromatic flarings in GRB 050904, 060210 and 080129 (the very late rebrightening in this burst) are the most likely candidates for a late jet - cocoon interaction event.

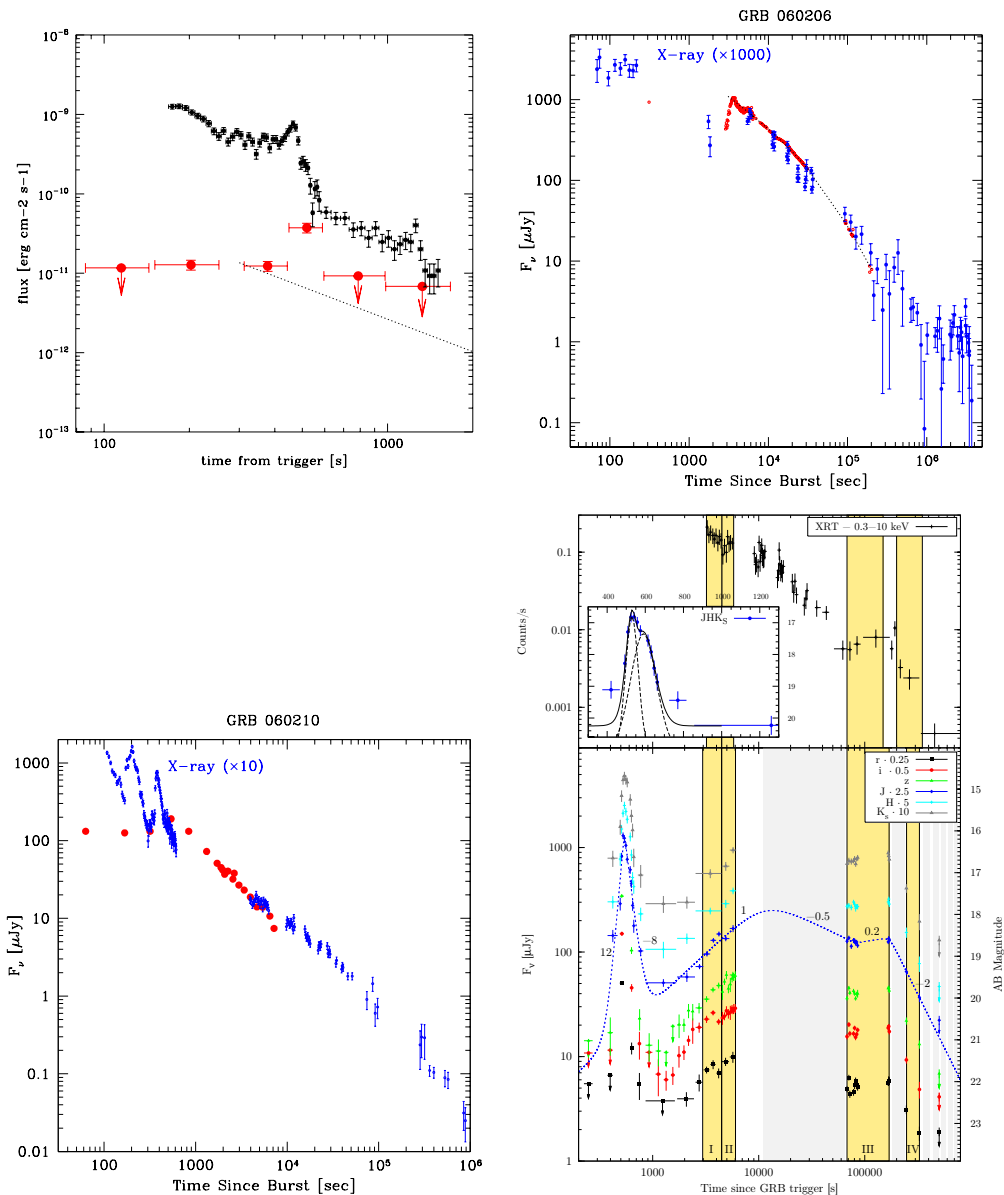


Figure 17. Four GRBs that show a late flare or rebrightening in optical afterglow light curve and, in cases where simultaneous X-ray observations are made, a contemporaneous X-ray flare. *Top left:* GRB 050904; filled circles in red are optical data and filled circles in black are X-ray data (from Boër et al. 2006). *Top right:* GRB 060206, and *bottom left:* GRB 060210; the open and filled circles in red color (with unnoticeable errors) are the optical data (from Stanek et al. 2007). *Bottom right:* GRB 080129 (from Greiner et al. 2009).

On the other hand, there are three cases in which simultaneous optical observations were available but no *optical* flare was detected at the time of very strong X-ray flare (the X-ray flux increased by factors ~ 100 in some of these cases), e.g., GRB 060418, 060607A (Molinari et al. 2007) and 060904B (Rykoff et al. 2009) which are shown in Fig. 18. This shows that not all X-ray flares are due to the late jet - cocoon interaction. However, neither the late jet nor the cocoon is ruled out in these three X-ray flares. The lack of an optical flare indicates that in these cases it is probable that a low-power, continuous jet with a luminosity of $L_{j,low}(t) = 2 \times 10^{48} t_1^{-2}$ erg s^{-1} (total energy \sim a few $\times 10^{49}$ erg) has kept the cavity open (see Section 4.2) and the internal shocks between the more powerful late jet and the preceding, slower, low-power jet gave rise to the X-ray flares.

6 SUMMARY

Observations of X-ray flares in many GRB afterglows suggest the existence of a late jet from a long-lived central engine of a GRB at $\sim 10^2$ s but possibly $10^4 - 10^5$ s after the main GRB event. Adopting the collapsing massive star origin for long-duration GRBs, and assuming that the supernova explosion to be at approximately the same time as the GRB, we have investigated the interactions of this late jet with the SNa ejecta and, with a cocoon that was left behind when the main GRB jet traversed the progenitor star.

We find that late jet - SNa ejecta interaction should produce a thermal transient, lasting about ~ 10 s and with a peak photon energy at a few keV, that should precede or accompany the flare. The luminosity of this transient is proportional to the kinetic luminosity of the late jet and can be as high as a few $\times 10^{48}$ erg s^{-1} . The lu-

minosity is smaller if the polar cavity created by the main GRB jet is only partially filled. This thermal transient is similar to the one associated with the breakout of the main GRB jet. Although it has a lower luminosity, its later occurrence makes it easier to detect. The observation of this signal can provide another evidence for the massive-star origin of GRBs and new information on the GRB - SNa association.

The fact that no such thermal transient was observed so far implies that the late jet - SNa ejecta interaction is suppressed. This could happen if the polar region of the ejecta was evacuated by the main GRB jet and cavity has not sufficiently refilled itself, especially for a not-too-late jet, e.g., $t_F \sim 10^2$ s, or the cavity could be kept open by a continuous, low-power jet. A strong thermal transient signal can also be blocked by the optically thick cocoon, which would be the case if the cocoon is slowly moving. An alternative possibility is of a failed supernova scenario in which the entire stellar envelope collapses in a free fall time of a few $\times 10^2$ s. In this case there is no supernova associated with the GRB and the late jet, if it is late enough, does not have to cross the stellar envelope.

The late jet interaction with the cocoon would cause a flare or rebrightening, superposed on the afterglow light curves, at both the optical and X-ray bands. This flare would have a pulse-width-to-time ratio $\Delta t/t < 1$ (the expected distribution of $\Delta t/t$ is similar to that for X-ray flares). Depending on model parameters, we find for a burst at a redshift $z = 2$ that the peak flux density at optical $f_{\nu_{opt}}$ ranges from 0.01 μJy to 0.1 Jy (V -band apparent magnitude 29 to 11.5) and at X-rays f_{ν_X} ranges from 0.001 μJy to 1 mJy. For typical parameters $f_{\nu_{opt}} \sim 0.1$ mJy (V -band magnitude ~ 19) and $f_{\nu_X} \sim 1$ μJy . Observational identification of this emission would verify the existence of the cocoon produced when the GRB jet traversed the progenitor star, thus it would be another confirmation of the collapsar model for long duration GRBs (e.g., MacFadyen & Woosley 1999; Ramirez-Ruiz et al. 2002; Matzner 2003; Zhang et al. 2004).

The late jet - cocoon interaction might have already been detected in four GRB afterglows in which simultaneous X-ray and optical flares with $\Delta t/t \ll 1$ were observed after the prompt emission has died off (see Fig. 17). From those candidate events, one can learn about the energetics of late jet and the cocoon by utilizing the emission calculation presented in this paper. Let us consider the flare event in GRB 050904 as an example. We find the most probable model parameters – for this burst at $z = 6.3$ and with $t_F = 70$ s – that produce the observed peak $f_{\nu_{opt}}$ and f_{ν_X} (data from Boër et al. 2006; Cusumano et al. 2007; Gou, Fox & Mészáros 2007) to be $E_c \approx 10^{51}$ erg, $\Gamma_c \approx 20 - 50$, $E_j \approx 10^{52}$ erg and $\Gamma_j \approx 500$. Those high energetics seem consistent with the very luminous nature of both the burst and the flare.

There are three cases in which no optical flare was detected at the time of a strong X-ray flare, even though a number of optical telescopes have been observing these bursts at the time of the X-ray flares (Fig. 18). This shows that not all X-ray flares are due to the late jet - cocoon interaction. However, neither a late jet nor the cocoon can be ruled out in these cases. It is possible that a low-power jet preceding the late jet with a total energy of at least 10^{49} erg had kept the cavity in the cocoon open, so that the late jet - cocoon interaction was suppressed. If correct this implies a low level continuous emission from the central engine at the level of $\sim 10^{47} (t/10 \text{ s})^{-2}$ erg s^{-1} lasting for $\sim 10^2$ s, assuming a radiation efficiency of ~ 0.1 .

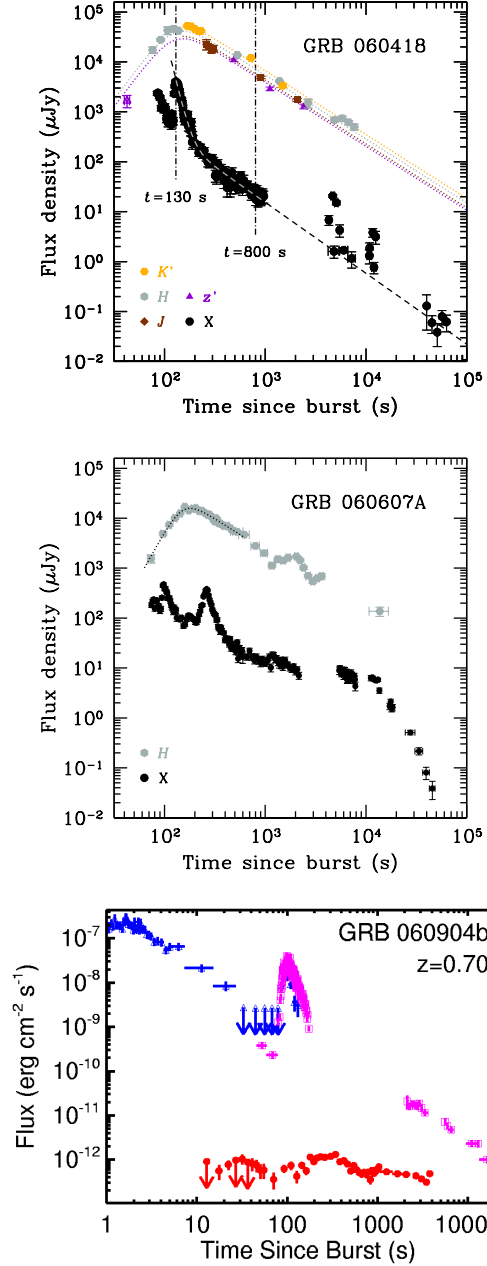


Figure 18. The three GRBs that show prominent late X-ray flares but without simultaneous optical flare apparent in the afterglow light curve. *Top:* GRB 060418; *Middle:* 060607a (both from Molinari et al. 2007). *Bottom:* GRB 060904b; blue triangles are BAT data extrapolated to X-ray band, magenta squares are XRT data and red circles are optical data (from Rykoff et al. 2009).

ACKNOWLEDGEMENT

RS is grateful to Craig Wheeler and Sean Couch for very helpful discussions. This work is supported in part by a NSF grant AST-0909110 (PK), and by an ERC advanced research grant and the ISF Center for High Energy Astrophysics (TP).

REFERENCES

- Barniol Duran R., Kumar P., 2009, MNRAS, 395, 955
- Blandford R. D., McKee C. F., 1976, Physics of Fluids, 19, 1130
- Bloom J. S. et al., 1999, Nature, 401, 453
- Bloom J. S. et al., 2002, ApJ, 572, L45
- Bloom J. S., Kulkarni S. R., Djorgovski S. G., 2002, AJ, 123, 1111
- Boër M., Atteia J. L., Damerdji Y., Gendre B., Klotz A., Stratta G., 2006, ApJ, 638, L71
- Böttcher M., Dermer C. D., 2000, ApJ, 532, 281
- Burrows D. N. et al., 2005, Science, 309, 1833
- Burrows D. N. et al., 2007, Phil. Trans. R. Soc. A, 365, 1213
- Campana S. et al., 2006, Nature, 442, 1008
- Castro Cerón, J. M. et al., 2006, ApJ, 653, L85
- Chincarini G. et al., 2007, ApJ, 671, 1903
- Christensen L., Hjorth J., Gorosabel J., 2004, A&A, 425, 913
- Cohen E., Piran T., 1999, ApJ, 518, 346
- Curran P. A. et al., 2007, A&A, 467, 1049
- Cusumano G. et al., 2007, A&A, 462, 73
- Della Valle M. et al., 2003, A&A, 406, L33
- Dermer C. D., 2008, ApJ, 684, 430
- Falcone A. D. et al., 2007, ApJ, 671, 1921
- Fan Y. Z., Wei D. M., 2005, MNRAS, 364, L42
- Fan Y., Piran T., 2006, MNRAS, 369, 197
- Fruchter A. S. et al., 2006, Nature, 441, 463
- Galama T. J. et al., 1998, Nature, 395, 670
- Gehrels N., et al., 2004, ApJ, 611, 1005
- Genet F., Daigne F., Mochkovitch, R., 2007, MNRAS, 381, 732
- Ghisellini G., Celotti A., Ghirlanda G., Firmani C., Nava L., 2007, MNRAS, 382, L72
- Goodman J. 1986, ApJ, 308, L47
- Gou L.-J., Fox D. B., Mészáros P., 2007, ApJ, 668, 1083
- Granot J., Königl A., Piran T., 2006, MNRAS, 370, 1946
- Granot J., Kumar P., 2006, MNRAS, 366, L13
- Greiner J. et al., 2009, ApJ, 693, 1912
- Hjorth J. et al., 2003, Nature, 423, 847
- Janka H.-Th., Langanke K., Marek A., Martínez-Pinedo G., Müller B., 2007, Physics Reports, 442, 38
- Katz J. I., Piran T., 1998, ApJ, 501, 425
- Katz J. I., Piran T., Sari R., 1998, Phy. Rev. Let., 80, 1580
- Kobayashi S., Zhang B., 2007, ApJ, 655, 391
- Kumar P., Granot J., 2003, ApJ, 591, 1075
- Kumar P., Narayan R., Johnson J. L., 2008, MNRAS, 388, 1729
- Landau L. D., Lifshitz E. M., 1959, Fluid Mechanics. Pergamon Press, Addison-Wesley Pub. Co., London, p. 501
- Lazzati D., Perna R., 2007, MNRAS, 375, L46
- Lazzati D., Perna R., Begelman M. C., 2008, MNRAS, 388, L15
- Li Z., Song L. M., 2004, ApJ, 608, L17
- MacFadyen A. I., Woosley S. E., 1999, ApJ, 524, 262
- Malesani D. et al., 2004, ApJ, 609, L5
- Matzner C., 2003, MNRAS, 345, 575
- McMahon E., Kumar P., Piran T., 2006, MNRAS, 366, 575
- Mészáros P., Laguna P., Rees M. J., 1993, ApJ, 415, 181
- Mészáros P., 2002, ARA&A, 40, 137
- Molinari E. et al., 2007, A&A, 469, L13
- Nakar E., Piran T., Granot J., 2003, New Astronomy, 8, 495
- Nakar E., Granot J., 2007, MNRAS, 380, 1744
- Nousek J. A. et al., 2006, ApJ, 642, 389
- O'Brien P. et al., 2006, ApJ, 647, 1213
- Paczynski B., 1986, ApJ, 308, L43
- Paczynski B., 1998, ApJ, 494, L45
- Panaitescu A., Mészáros P., Burrows D., Nousek J., Gehrels N., O'Brien P., Willingale R., 2006, MNRAS, 369, 2059
- Pe'er A., Mészáros P., Rees, M. J., 2006, ApJ, 652, 482
- Piran T., Shemi A., Narayan R., 1993, MNRAS, 263, 861
- Piran T., 1999, Physics Reports, 314, 575
- Piran T., 2005, Rev. Mod. Phys., 76, 1143
- Piro L. et al., 1998, A&A, 331, L41
- Ramirez-Ruiz E., Celotti A. & Rees M. J., 2002, MNRAS, 337, 1349
- Rybicki G. B., Lightman A. P., 1979, Radiative Processes in Astrophysics. Wiley-Interscience Press, New York.
- Rykoff E. S. et al., 2009, ApJ, 702, 489
- Sari R., Piran T., Narayan R., 1998, ApJ, 497, L17
- Sari R., Piran T., 1999, ApJ, 520, 641
- Shemi A., Piran T., 1990, ApJ, 365, L55
- Shen R.-F., Zhang B., 2009, MNRAS, 398, 1936
- Stanek K. Z. et al., 2007, ApJ, 654, L21
- Tanaka M. et al., 2009, ApJ, 692, 1131
- Uhm Z. L., Beloborodov A. M., 2007, ApJ, 665, L93
- Woosley S. E., Bloom J. S., 2006, ARA&A, 44, 507
- Woosely S. E., Heger A., 2006, in Holt S. S., Gehrels N., Nousek J. A., eds, AIP Conf. Proc. Vol. 836, Gamma Ray Bursts in the Swift Era, American Institute of Physics, Melville, NY, p. 398
- Woźniak P. R., Vestrand W. T., Wren J. A., White R. R., Evans S. M., Caspersen D., 2006, ApJ, 642, L99
- Wheeler C. J., Yi I., Höflich P., Wang L., 2000, ApJ, 537, 810
- Wheeler C. J., Meier D. L., Wilson J. R., 2002, ApJ, 568, 807
- Yu Y. W., Dai Z. G., 2007, A&A, 470, 119
- Yu Y. W., Dai Z. G., 2009, ApJ, 692, 133
- Zhang B., Mészáros P., 2001, ApJ, 552, L35
- Zhang B., 2006, Advances in Space Research, 40, 1186
- Zhang W., Woosley S. E., Heger A., 2004, ApJ, 608, 365